A channeled spectro-polarimeter for ground based atmospheric monitoring

Master's thesis in Wireless, Photonics and Space engineering

JOHAN ALBRÅTEN

DEPARTMENT OF SPACE, EARTH AND ENVIRONMENT

Chalmers University of Technology
Gothenburg, Sweden 2025
www.chalmers.se

Master's thesis 2025

A channeled spectro-polarimeter for ground based atmospheric monitoring

JOHAN ALBRÅTEN

CHALMERS
UNIVERSITY OF TECHNOLOGY

Department of Space, Earth and environment
Division of Geoscience and Remote Sensing
Chalmers University of Technology
Gothenburg, Sweden 2025

A channeled spectro-polarimeter for ground based atmospheric monitoring

JOHAN ALBRÅTEN

© JOHAN ALBRÅTEN, 2025.

Supervisor: Santiago Arellano, Department of Space, Earth and Environment, Chalmers.
Examiner: Johan Mellqvist, Department of Space, Earth and Environment, Chalmers.

Master's Thesis 2025
Department of Space, Earth and Environment
Division of Geoscience and Remote Sensing
Chalmers University of Technology
SE-412 96 Gothenburg
Telephone + 46 (0)31-772 1000

Typeset in LaTeX
Gothenburg, Sweden 2025

A channeled spectro-polarimeter for ground based atmospheric monitoring

Johan Albråten

Department of Space, Earth and Environment
Division of Geoscience and Remote Sensing
Chalmers University of Technology

Abstract

Characterization of particle content in the atmosphere can be of both public health- and scientific interest. One way of characterizing the particle content, without the need of having the Sun behind the target, is by analyzing the polarization of the light incident from the direction of interest. This project has entailed the assembly and testing of a polarimeter capable of detecting the presence of varying particle content in the atmosphere, with high wavelength resolution. A detailed account of this process is described in this document, including some theoretical background to facilitate interpretation of the results. The principle of operation is similar to some existing instruments but adapted for practical inclusion into the volcanic monitoring network NOVAC, or other ground based enterprises such as monitoring of pollution in urbanized areas. Some work remains to scope the capacity of the instrument, but the basic capability has been verified.

Acknowledgement

This project was conceptualized and made possibe through my supervisor Santiago Arellanos's affiliation with NOVAC. He also provided valuable feedback on the report, good discussions of the project direction and practical support in working with the NOVAC hardware. Access to the lab at the Space, Earth and Environment department and the 3d-printers at the CASE-lab at Chalmers was also essential.

Contents

1 Background

1.1 Introduction and project overview

Light incident on Earth from the Sun scatters on particles as it passes through the atmosphere. For each scattering event the mechanism depends on attributes of both the incident light and the particle. One possible consequence of scattering events is a fractional increase (or decrease) of the coherent oscillation of the light; its polarization. The light scattered from the sky towards an observer on the ground has some degree of polarization under all weather conditions. The fact that the degree of polarization is particle dependent can be used to identify the particle content of the space that the light has traversed, to some degree.

This document describes the process of assembling an instrument capable of identifying the degree of polarization of scattered light and to identify polluting particle content by its effect on polarization, specifically in a high resolution, wavelength separated manner.

There exists a vast range of instruments capable of detecting polarization. The specific aim of this work has been to develop a working prototype similar to some existing systems such as the satellite-based SPEXone [**1**, **2**] and the ground-based GroundSPEX [**3**] for later development and potential use in the *Network for Observation of Volcanic and Atmospheric Change* [NOVAC] [**4**]. The instruments mentioned detect the degree of linear polarization of light scattered from the atmosphere. The difference between these examples and the polarimeter of the instrument of this project will be discussed further down in the document.

A short theoretical description of polarization and scattering theory is presented further ahead in this section to facilitate further reading. Thereafter follows a detailed description of how the instrument works in theory and how this functionality was verified through a number of lab- and field tests. The results of each test is presented together with the test description. The results are then summarized and discussed in the "Conclusion" section. Lastly, some ideas for future development are discussed.

1.1.1 Limitations

- Project duration: 4-5 months.
- Test equipment: At the time of testing, access to a particle sizer/ electron microscope or equivalent equipment to characterize test targets (smoke particles) accurately, was not practical and priority was given to moving the tests along since it was still possible to get relevant test results. Estimation of particle size distribution and shape was guessed by referencing relevant experiments described in literature.
- Field targets: The time available for measurements at each site was limited in both a practical and financial sense. This was because the search for suitable smoke plumes took time and use of a rental car. Suitable industrial areas were thereafter found a few hours drive from Gothenburg. This limited the possibility to redo measurements if a mistake or data corruption was discovered during the data processing stage, to a few times.

- It was important to test basic functionality of the instrument with well defined targets and as little influence of confounding factors as possible. This meant that it was necessary to have mostly clear skies at the right time of day. For practical reasons, this also limited the time available for measurements.

1.2 Basic concepts

1.2.1 Polarization

Light propagating through space can be visualized as a wave of energy that oscillates perpendicularly to its direction of propagation. It consists of a magnetic and electric field component, oriented orthogonally to each other. Generally speaking, the electric field is stronger and dominates in the interaction with matter in the way that is relevant to this theory. The direction of the oscillation can further be described by the angular direction it has in a plane, oriented perpendicularly to the direction of propagation. This angle thus lies in the range $[0^o\ 360^o]$. The direction of the wave crest in each plane at a given point in time can also be phase dependent. Light from the Sun, incident on the atmosphere, is mostly unpolarized, meaning that the wave seem to oscillate randomly in all directions over time. This is typically because the unpolarized wave consists of a superposition of waves with different polarization states with completely random phase relative to each other. This is due to the statistically very widespread orientation of the source contributors as well as their typically very short duration emissions [**5**, **6 (ch.8.1.4)**]. There are five additional descriptive states of polarization: Linear, right- and left-handed circular, right- and left handed elliptical. Generally speaking, linear and circular polarizations are extreme cases of elliptical polarization:

Linear: The light oscillates along a line in the observation plane, penetrating the origin.

Right handed circular: With the thumb of the right hand in the direction of propagation, the direction of oscillation turns around the observation plane in a circular fashion along the direction of the other fingers. The rotation rate is constant throughout the cycle. The angle is phase dependent.

Left handed circular: Similar to right handed circular but orientation can be visualized with the thumb of the left hand in the direction of propagation.

Right handed elliptical: With the thumb of the right hand in the direction of propagation, the direction of oscillation turns around the observation plane in an elliptical fashion along the direction of the other fingers. The rotation rate is cyclical throughout the cycle. The angle is phase and semi-major axis dependent.

Left handed elliptical: Similar to right handed elliptical but orientation can be visualized with the thumb of the left hand.

The angle of the polarization has a certain distribution pattern in relation to the sun for an observer on the ground and this pattern typically does not vary with the weather unless the sky is heavily overcast, with limited direct illumination of the scattering particles. The degree of polarization is highly weather dependent however [**7**, **8**].

1.2.2 Stokes parameters

The Stokes parameters are mathematical representations of the polarization state that, among other things, can be useful for visualization. They will be used to illustrate the functionality of the instrument further ahead in the document, so are here defined for reference [**6 (ch.8.13)**].

- S_o, total intensity of beam.
- S_1, horizontal- vs vertical linear polarization.
- S_2, $+45^o$ linear vs -45^o degree of linear polarization.
- S_3, degree of circular polarization (left vs right).

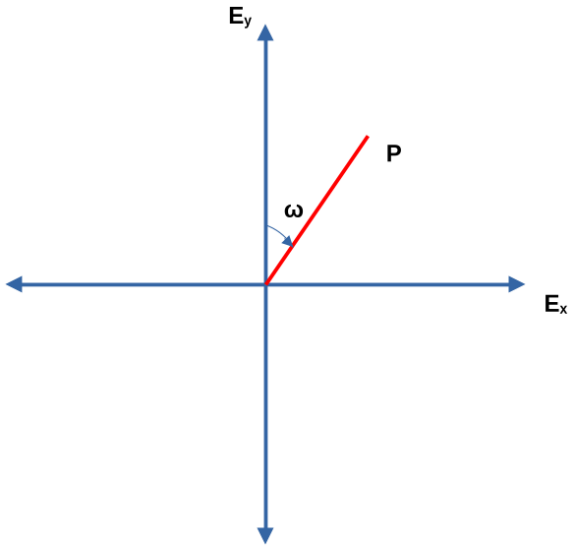

Figure 1: Representation of orthogonal components of polarized light E_y and E_x. P illustrates the direction of the polarization. ω is the angle of polarization as measured clockwise from the positive y-axis.

Let E_P denote the electric field in a direction of angle ω in the observation plane. Then, using the geometry of figure 1, we get the relation:

$$E_P = |E_y|\cos(\omega) + i|E_x|\sin(\omega) \tag{1}$$

The intensity of the light wave can be written as:

$$I = E_P E_P^\star \tag{2}$$

where * annotates the complex conjugate. The normalized Stokes parameters can be written out as:

$$S_o = (E_x E_x^\star + E_y E_y^\star)/I \tag{3}$$

$$S_1 = (E_x E_x^\star - E_y E_y^\star)/I \tag{4}$$

$$S_2 = (2E_x E_y^\star \cos(\omega))/I \tag{5}$$

$$S_3 = (2E_x E_y^\star \sin(\omega))/I \tag{6}$$

Methods to measure the Stokes parameters can be found in many resources, for instance from Collet. E (1984) [**9**]: By rotating a linear polarization filter to $\theta = 0^o$ the y-component can be eliminated. By rotating the filter to $\theta = 90^o$ the x-component can be eliminated. In this way we can get S_o and S_1. At a rotation angle of 45^o we get:

$$I_{45^o} = ((E_y + E_x)/\sqrt{2})((E_y^\star + E_x^\star)/\sqrt{2}) = I((S_o + S_2)/2) \tag{7}$$

And by already knowing S_o we can retrieve S_2. By using a quarter wave retarder the intensity can be written as:

$$I_{45^o,\lambda/4} = I(S_o + S_3)/2 \tag{8}$$

Like for S_2, S_3 can then be inferred. For mathematical operations, the parameters can be ordered into a *Stokes vector* that looks like this:

$$S = \begin{bmatrix} S_0 \\ S_1 \\ S_2 \\ S_3 \end{bmatrix} \tag{9}$$

When referring to the parameters further into the document, the values will be normalized by intensity and so have values between -1 and 1.

The effect of optical components on the polarization of incident light can be described by mathematical operations on the Stokes vector. This operation can be in the form of matrix multiplication with a so called Mueller matrix, lets denote it by M_{comp}. The elements of each Mueller matrix are attenuation factors specific for the effect of the component on the Stokes parameter multiplied by it. Lets say the system contains three optical components and the stokes vector of the incident and transmitted light is S_i and S_t respectively, the operation then becomes:

$$S_t = M_{\text{comp3}} M_{\text{comp2}} M_{\text{comp1}} S_i \tag{10}$$

1.3 Scattering of light

1.3.1 Atmospheric scattering and polarization

As mentioned previously, the mechanism of atmospheric scattering depends on properties of both the incident light and the particle.

When particles are at least ten times smaller than the wavelength of the light, the wave can cause secondary radiation, released by oscillations of the electrons of the particle, in an isotropic fashion.

This is called Rayleigh scattering [**6 (ch.4.2)**]. The mechanism produces linearly polarized light. At a right angle from the incoming light, light scattered in this way is expected to be completely linearly polarized for the single-source-single-scattering case.

For particles or structures of a spherical shape, such as droplets, that are about equal size of the wavelength of the light, the scattering can be described by so called Mie-theory. The mechanism is somewhat similar to Rayleigh scattering but the re-radiation profile is not as isotropic and the highest intensity is radiated along the original propagation direction of the incident light [**10**]. For irregular particles of this size there are different models that can simulate the scattering pattern, which can have a vast range of profiles, but still have a profile reminiscent of the rayleigh scattered light [**11**].

The light reaching the ground is not completely polarized, even at a right angle from the incident sunlight. This is due to multiple scattering, the anisotropy of air molecules, reflection on surfaces, non-symmetric scattering mechanisms, geometric scattering of larger particles, and secondary light sources, such as anthropogenic light, fluorescence, etc. The polarized component of the sky light consists of mainly linear polarization. Circular polarization is not common in nature and the component of sky light that is elliptically polarized seem to be insignificant under normal conditions [**12**, **13**].

The intensity of the Rayleigh scattering is much more wavelength dependent than for Mie scattering. For both mechanisms the wavelength of the incident and re-radiated light are the same. These two mechanisms are the main cause of the polarization of the light scattered to an observer on the ground. In clear skies Rayleigh scattering dominates and Mie/geometric scattering is more dominant for overcast skies and low elevation light transmission. There are a few more types of scattering of which only the geometric scattering of particles much larger than the wavelength of the incident light will be mentioned here.

1.3.2 Rayleigh polarization model

It has been found that the degree of polarization of Rayleigh scattered light largely follows the distribution described by [**14**]:

$$P = \frac{\sin^2(\theta)}{1 + \cos^2(\theta) + 2\delta/(1-\delta)} \tag{11}$$

where θ is the angle between the Sun and the point of interest from the observer or the *scattering angle* and δ is the so called depolarization factor, which is gas-specific ratio of typical fraction of intensity of light polarized perpendicular and parallel to the scattering plane (for air it is typically 0.03) [**15**]. Since the polarization's angular distribution profile is similar for overcast and clear skies, the model is considered valid for overcast skies, for which Mie scattering is more dominant, as well. There may be deviations in degree of polarization spot-wise in partly cloudy or heavily polluted skies. Figure 2 illustrates the geometry and figure 3 displays the shape of the polarization distribution by scattering angle according to this model.

It then follows that to calculate the expected polarization profile at a given point in time one must determine both the position of the sun and the position of the target in relation to the instrument.

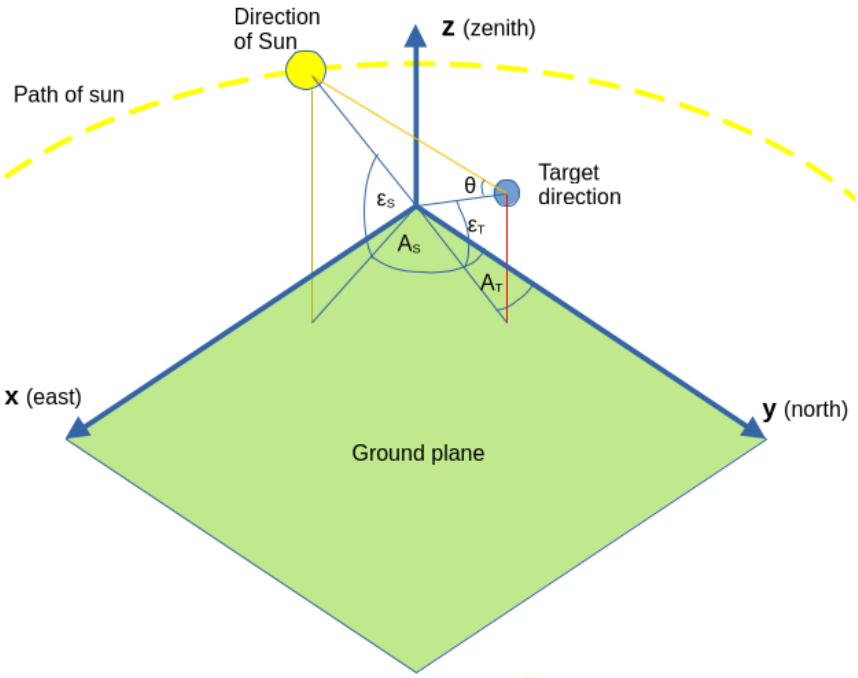

Figure 2: Geometry of observations. The instrument is located at the origin. A_T and A_S represents the azimuth of the target and Sun respectively. Similarly ϵ_T and ϵ_S represents their elevations.

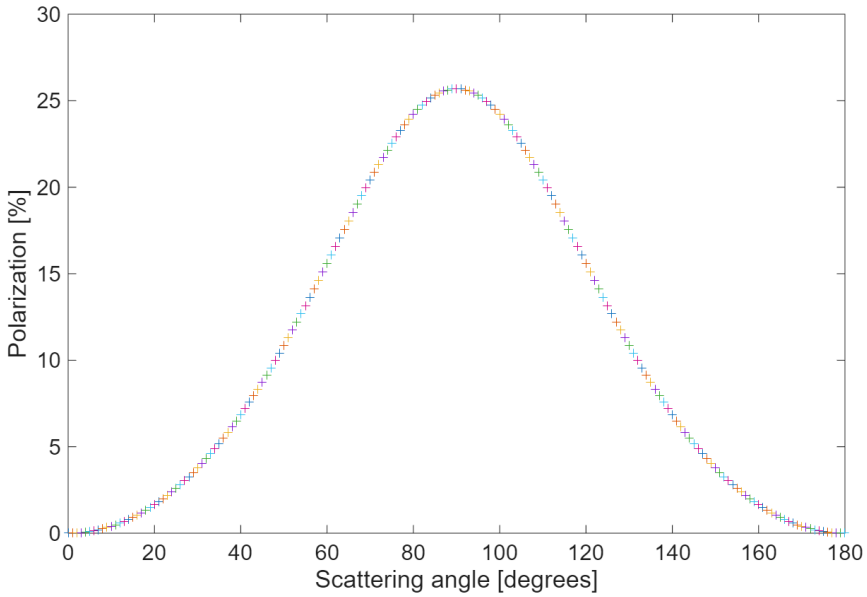

Figure 3: Polarization curve in relation to scattering angle according to the Rayleigh model (arbitrary degree of polarization).

The instrument is intended for stationary use so the reference point on the ground is fixed. The scattering is fairly simple to describe if the target is on the plane mapped by the observer, zenith and the sun (the principal plane).

The attributes that are relevant to interpret the retrieved data correctly are displayed in the following list for clarity:

- The date and time of day t.
- The azimuth of the target plane $A_T = A_T(t)$
- The elevation of the target $\epsilon_T = \epsilon_T(t)$
- The azimuth of the sun $A_S = A_S(t)$
- The elevation of the sun $\epsilon_S = \epsilon_S(t)$

These then give us the scattering angle, $\theta = \theta(A_T, \epsilon_T, A_S, \epsilon_S)$.

2 Instrument description

In this section the light manipulation of the polarimeter is explained. The final mounting, direction, control and data read of the polarimeter will be discussed in the "Incorporation into NOVAC-equipment"-section. Different temporary setups were used for different lab tests, these will be described in the "Lab test"-sections.

2.1 Principle of operation

Light with any state of polarization is incident on the optical interface depicted schematically in figure 5 (the components are described in more detail in table 3 of the following section). The fast axis of the Fresnel rhomb quarter wave retarder is oriented vertically in the figure. Linearly polarized light oriented along the fast axis of the Fresnel rhomb will pass this component unchanged in polarization. Light polarized 45^o from the fast axis will become left- or right handed circularly polarized, depending on if the deviation is clockwise or counterclockwise. Light polarized perpendicularly to the fast axis will be phase delayed but not change its state of polarization. All other directions of linearly polarized light will undergo varying degrees of elliptical polarization. Circularly polarized light will emerge as linearly polarized light oriented $\pm 45^o$ from the fast axis depending on the handedness of the initial polarization. Elliptically polarized light will undergo a rotation of its main axis of polarization and possibly change its ellipticity.

Next, light enters the multiple order quarter wave retarder with its fast axis oriented 45^o clockwise from the fast axis of the Fresnel rhomb, as viewed from the multiple order retarder towards the Fresnel rhomb. The effect on the light here is similar to what was described for the Fresnel rhomb above. The difference is that the quarter wave effect comes into play cyclically as $n * \lambda/4$ times for the spectrum while the wavelengths in between are retarded by varying fractions of a quarter wavelength. Table 1 gives an overview of the different polarization paths through the components.

After the multiple order retarder, the output signal is retrieved after it has passed a polarizing beam splitter with its fast axis oriented vertically. A difference between this instrument and the SPEXone or groundSPEX, in regards to its basic functioning principle, is that only the vertical component of the light emerging from the multiple order retarder is retrieved for analysis (in the mentioned instruments, both the vertical and horizontal components are retrieved). The output will have a cyclically varying shape; a so called modulation pattern. The modulation pattern is created because the component of the light output from the multiple order retarder that has an angle of polarization equal to the beam splitter output varies cyclically, according to the phase of the retardation in the multiple order retarder. Unpolarized light passes through unaffected and thus can create an intensity body that does not have a modulation pattern, in the output spectra. The intensity of incident linearly polarized light is roughly equal to the relative magnitude of the modulation pattern as a fraction of the total signal. Circularly polarized light, incident on the polarimeter, will enter the multiple order retarder as linearly polarized light oriented along its fast axis or rotated by ninety degrees from it, dependent on the initial handedness. This means that it will later be split into two equal components by the beam splitter and that this signal will be equal for both the horizontal and vertical retrieval paths. Since linearly polarized light has a constant angle of polarization it will contribute far less to the modulation pattern, even if the angle is slightly off axis in the multiple order retarder, than the light that is circularly or elliptically polarized when incident on

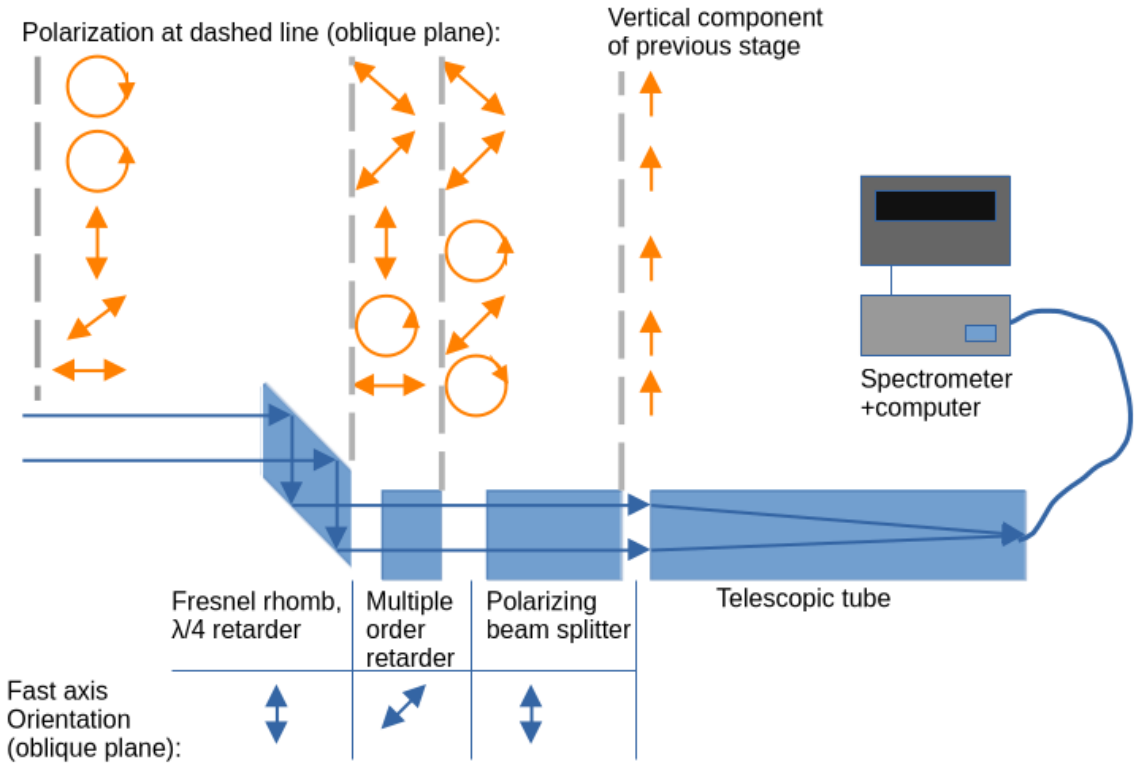

Figure 4: Enter Caption

Figure 5: Schematic overview of the polarimeter and effect on some examples of the polarization state at each stage. The components are further described in table 3.

the multiple order retarder (that is linear or elliptically polarized when incident on the polarimeter).

Table 1: Polarization stage of light after the given stages of the path. Positive value of the orientation of polarization is meant as clockwise from the perspective of the receiver. For the multiple order retarder the effect is valid for those wavelengths where it has a quarter wave retardation effect. ϕ indicates a phase shift independent of the polarization state.

Stage	**Polarization state**					
Incident light	Linear 0^o	Linear 90^o	Linear $\pm 45^o$	Linear other ω	Elliptical	Left/right handed circular
Fresnel rhomb	Linear 0^o	Linear 90^o $\phi : +90^o$	Left/right handed circular	Elliptical	Elliptical trans-formed	Linear $\pm 45^o$
Multiple order retarder at $+45^o$	Right handed circular	Left handed circular	Cyclically $90^o/0^o$ linear	Elliptical trans-formed	Elliptical trans-formed again	Linear $\pm 45^o$ $\phi : 0^o/90^o$
Beam splitter	$0^o(0-50\%)$ - fraction	$0^o(0-50\%)$- fraction	$0^o(0-100\%)$- fraction	$0^o(0-x\%)$- fraction	$0^o(0-x\%)$- fraction	$0^o(50\%)$- fraction

A theoretical description for what happens in the polarimeter can also be made by using Mueller matrices as was mentioned previously. The following representation assumes ideal athermal and achromatic components respectively [**16 (p.41)**, **17**]:

$$M_{\mathrm{MOR}}M_{\mathrm{FR}} = \underbrace{\begin{bmatrix} 1 & 0 & 0 & 0 \\ 0 & \cos(2\pi\delta/\lambda) & 0 & -\sin(2\pi\delta/\lambda) \\ 0 & 0 & 1 & 0 \\ 0 & \sin(2\pi\delta/\lambda) & 0 & \cos(2\pi\delta/\lambda) \end{bmatrix}}_{\textbf{Multiple order retarder}} \underbrace{\begin{bmatrix} 1 & 0 & 0 & 0 \\ 0 & 1 & 0 & 0 \\ 0 & 0 & 0 & -1 \\ 0 & 0 & 1 & 0 \end{bmatrix}}_{\textbf{Fresnel rhomb}} = \tag{12}$$

$$= \underbrace{\begin{bmatrix} 1 & 0 & 0 & 0 \\ 0 & \cos(2\pi\delta/\lambda) & -\sin(2\pi\delta/\lambda) & 0 \\ 0 & 0 & 0 & -1 \\ 0 & \sin(2\pi\delta/\lambda) & \cos(2\pi\delta/\lambda) & 0 \end{bmatrix}}_{\textbf{Polarimeter transformation}} = M_{\mathrm{T1}}$$

For the general Stokes vector, the output from the polarimeter (before the beam splitter) becomes as follows:

$$M_{\mathrm{T1}}S = \begin{bmatrix} 1 & 0 & 0 & 0 \\ 0 & \cos(2\pi\delta/\lambda) & -sin(2\pi\delta/\lambda) & 0 \\ 0 & 0 & 0 & -1 \\ 0 & \sin(2\pi\delta/\lambda) & \cos(2\pi\delta/\lambda) & 0 \end{bmatrix} \begin{bmatrix} S_0 \\ S_1 \\ S_2 \\ S_3 \end{bmatrix} = \tag{13}$$

$$= \begin{bmatrix} S_0 \\ \cos(2\pi\delta/\lambda)S_1 - \sin(2\pi\delta/\lambda)S_2 \\ -S_3 \\ \sin(2\pi\delta/\lambda)S_1 + \cos(2\pi\delta/\lambda)S_2 \end{bmatrix}$$

In reality the wavelength independence of the Fresnel rhomb and the thermal independence of the multiple order retarder is not perfect and actual Mueller matrix measurements need to be made if one wants to make the most accurate representation (an example for reference can be found in Honggang Gu et al. 2018 [**18**]). Other factors that can influence that actual transformation are attenuation factors, air gaps between interfaces, minor alignment errors, etc. Previous measurement results for the Mueller matrices of the exact components are not available according to staff contacted at the manufacturer's and making measurements within this project would be beyond its intended scope (this could be something to consider for future development).

To describe the actual measured output signal, it is possible to use the Mueller matrix of the polarizing beam splitter (in vertical orientation) [**17**]:

$$M_{\mathrm{BS}} = 1/2 \begin{bmatrix} 1 & 1 & 0 & 0 \\ 1 & 1 & 0 & 0 \\ 0 & 0 & 0 & 0 \\ 0 & 0 & 0 & 0 \end{bmatrix} \tag{14}$$

Which, multiplied with the transformation matrix of the previous steps. gives us the output:

$$S_{\mathrm{out}} = M_{\mathrm{BS}}M_{\mathrm{MOR}}M_{\mathrm{FR}}S = 1/2 \begin{bmatrix} S_0 + \cos(2\pi\delta/\lambda)S_1 - \sin(2\pi\delta/\lambda)S_2 \\ S_0 + \cos(2\pi\delta/\lambda)S_1 - \sin(2\pi\delta/\lambda)S_2 \\ 0 \\ 0 \end{bmatrix} \tag{15}$$

Using that $I_a S_{\mathrm{out}}(1,1)$ (I_a being the incident intensity) can be set to equal the output intensity and that the Stokes parameters themselves can be manipulated to produce the angle of polarization and degree of linear polarization, an equation can be derived to extract the degree of polarization from measured quantities. The equation has been derived and presented in various recources, for instance by Snik et al, 2009 ([**19**]). The full derivation will be made for the instrument specific analysis in section 5. Here the equation valid for the theory so far and for the initial lab tests, is simply presented to save space:

$$I_{\perp/||} = \frac{I_a(\lambda)}{2}(1 \pm P(\lambda)\cos(\phi(\lambda))) \tag{16}$$

$$\phi = \frac{2\pi\delta(\lambda)}{\lambda} + 2\omega(\lambda) \tag{17}$$

Here $I_{\perp/||}$ are the orthogonal components of the output intensity, equal to half of the maximum fitted intensity at that wavelength, P is the degree of polarization as a fraction of one, δ is the total angular retardation of the system and ω is the angle of linear polarization. Note that the modulation pattern mentioned previously in this section is determined in amplitude by P and in phase by ϕ. The sought after output information is:

$$\pm P(\lambda) = \frac{1}{\cos(\phi(\lambda))} \left(\frac{2I(\lambda)}{I_a(\lambda)} - 1 \right) \tag{18}$$

In table 2 the calculated effect of the polarimeter on different polarization states of the incident light, using Mueller matrices and Stokes vectors (using equation 10), are listed. The result of the matrix multiplication seem to be similar to what is expected from previously stated theory summarized in table 1.

Table 2: Mathematical representation of polarizers effect on the polarization of the passing light, before it enters the beam splitter.

Polarization of incident light	**Stokes vector of incident light**	**Stokes vector of transmitted light**	**Polarization of transmitted light**
Linear vertical	$\begin{bmatrix} 1 \\ -1 \\ 0 \\ 0 \end{bmatrix}$	$\begin{bmatrix} 1 \\ -\cos(2\pi\delta/\lambda) \\ 0 \\ \sin(2\pi\delta/\lambda) \end{bmatrix}$	Cyclically right circular
Linear horizontal	$\begin{bmatrix} 1 \\ 1 \\ 0 \\ 0 \end{bmatrix}$	$\begin{bmatrix} 1 \\ \cos(2\pi\delta/\lambda) \\ 0 \\ -\sin(2\pi\delta/\lambda) \end{bmatrix}$	Cyclically left circular
Linear 45^o	$\begin{bmatrix} 1 \\ 0 \\ 1 \\ 0 \end{bmatrix}$	$\begin{bmatrix} 1 \\ -\sin(2\pi\delta/\lambda) \\ 0 \\ \cos(2\pi\delta/\lambda) \end{bmatrix}$	Cyclically linear vertical
Left circular	$\begin{bmatrix} 1 \\ 0 \\ 0 \\ -1 \end{bmatrix}$	$\begin{bmatrix} 1 \\ 0 \\ 1 \\ 0 \end{bmatrix}$	Linear 45^o
Right circular	$\begin{bmatrix} 1 \\ 0 \\ 0 \\ 1 \end{bmatrix}$	$\begin{bmatrix} 1 \\ 0 \\ -1 \\ 0 \end{bmatrix}$	Linear -45^o
Arbitrary elliptical	$\begin{bmatrix} 1 \\ 0.4 \\ 0.7 \\ 0.8 \end{bmatrix}$	$\begin{bmatrix} 1 \\ 0.4\cos(2\pi\delta/\lambda) - 0.7\sin(2\pi\delta/\lambda) \\ -0.8 \\ 0.4\sin(2\pi\delta/\lambda) + 0.7\cos(2\pi\delta/\lambda) \end{bmatrix}$	Elliptically transformed
Arbitrary linearly polarized	$\begin{bmatrix} 1 \\ 0.6 \\ 0.7 \\ 0 \end{bmatrix}$	$\begin{bmatrix} 1 \\ 0.6\cos(2\pi\delta/\lambda) - 0.7\sin(2\pi\delta/\lambda) \\ 0 \\ 0.6\sin(2\pi\delta/\lambda) + 0.7\cos(2\pi\delta/\lambda) \end{bmatrix}$	Elliptically polarized
Unpolarized	$\begin{bmatrix} 1 \\ 0 \\ 0 \\ 0 \end{bmatrix}$	$\begin{bmatrix} 1 \\ 0 \\ 0 \\ 0 \end{bmatrix}$	Unpolarized

2.2 Polarimeter hardware

The components used are listed in table 3. Reference documentation for the spectrometer could not be readily found online; if one wants to delve into details they can contact the manufacturer or refer to documentation of similar spectrometers from the same manufacturer.

Table 3: Main components of polarimeter, listed in order.

Component	**Specifics**	**Description**
$\lambda/4$ retarder	Thorlabs mounted Fresnel Rhomb 1/4W [**20**].	Chrystal which introduce a 90 degree phase shift of the incident light by means of internal reflection. This specific component is achromatic, meaning that it has an equal effect for different wavelengths.
Multiple order $\lambda/4$ retarder	From B.Halle, Quartz 1.63 mm. MgF2 3.82mm. 400-900nm. Custom made previously for groundSpex. Athermal. Order=43, Similar at [**21**].	Functions as a quarter wave retarder, but cyclically, over the spectra. Mechanism is a wavelength-dependent optical thickness of the material.
Polarizing beamsplitter	Thorlabs GTH10M. [**22**]	Splits the incoming light into two orthogonally polarized components, allowing one of them to pass through.
Telescope	Made in-house, plane-convex lens to fiber	A hollow tube with a plane-convex lens of focal length 5 cm in one end and a connection for an optical fiber in the other end, coinciding with the focal length.
Spectrometer	Ocean Optics, S2000 CCD detector, spectral resolution of 0.5 nm, wavelength range of 350 to 550 nm.	Receives light and separates the signal in to different wavelength channels. The intensity is then stored.

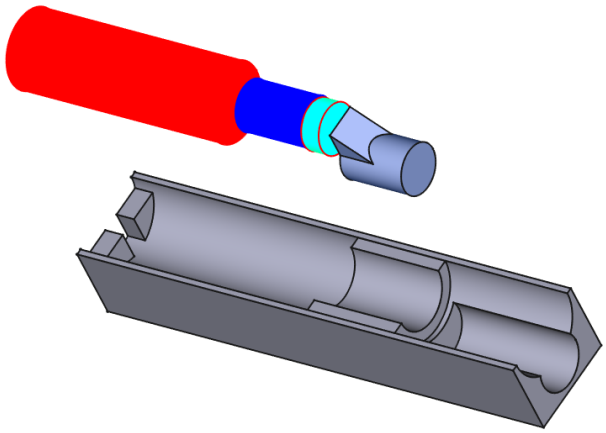

Figure 6: CAD-schematic of mount for lab tests, in preparation for 3d printing. The mount itself is colored gray while the optical components are displayed as a train above. Red: telescopic tube, blue: polarizing beam splitter, teal: multiple order retarder, metallic blue: Fresnel-rhomb.

3 Lab tests part 1: components

A number of experiments were performed on each component and on the system as a whole. This was done partly as tests of functionality but also as exercises to achieve some familiarization with equipment and components. Some experiments are presented here because they illustrate the functionality of the components in a useful manner and also serve to provide introduction to system tests further down in the document. In the images a specific type of 3d-printed rack can be seen. A few different rack-designs were made and printed and used throughout the test-stages.

3.1 Lightpath alignment

The light path alignment was secured through alignment of the respective component casings, which were overall well enough fitted in the 3d-printed racks for the accuracy sought after.

3.2 Generation of partially polarized light

The simplest way to generate linearly polarized light is to pass light of any polarization through a polarizing filter, setup with the sought after orientation. When experiments were to start, a separate polarization filter was not readily at hand, so instead testing commenced by using light reflected at the Brewster angle as a polarized source [**6 (ch.8.6)**]. The light source used throughout the lab-tests were a Xenon lamp which produces unpolarized light with high intensity. Later a polarization filter was found but the tests yielded some unexpected illustrative results, so it was decided to include the tests using the Brewster angle here. When light is incident on a semitransparent material in the Brewster angle, the light component with polarization parallel to the surface will be completely reflected while other components pass through. Since the generation of polarized light using this method was very inexact, we also got a fraction of unpolarized light, which incidentally created a signal with similar composition as what would be expected for field measurements.

The Brewster angle is given by:

$$\alpha_B = \arctan(n_{\text{crystal}}(\lambda)/n_{\text{air}}(\lambda)) \tag{19}$$

Where n_{crystal} and n_{air} denotes the refractive indices of glass and air respectively.

If one aligns the instruments with high accuracy to capture light reflected at this angle, as the polarizing beam splitter is rotated, an increase in spectral intensity should be observed around the direction parallel to reflective surface.

As mentioned previously, the spectrometer used covers an interval between 350 nm and 550 nm, with the bulk of the light from the xenon-lamp producing high intensity spectra between 430 nm and 510 nm. Here the refractive index of the quartz crystal is expected to vary between 1.4672 and 1.4618 [**23**]. For air the corresponding change is 100 times less. This corresponds to an interval of the Brewster angle of:

$$\alpha_B = [55.62^o, 55.72^o] \tag{20}$$

The equipment available did not facilitate this level of exactness, so some minor deviation from the Brewster angle, up to a few degrees, was by necessity accepted for the experiments.

3.2.1 Procedure and result

Procedure: The setup is shown in figure 7. The Xenon lamp was turned on for at least 30 minutes before measurements commenced. A semitransparent quartz crystal, cut in a shape of a 1 cm thick cylinder, was mounted in a way so that light passing through it would not be reflected back from the rack holding the crystal. Using a protractor, the light from the xenon-lamp was made to fall towards the crystal in the Brewster angle. Using a 3d printed mount, a beam splitter was placed in front of a telescopic tube and oriented along the Brewster angle on the other side of the crystal normal. Since the crystal was mounted vertically the reflected light was expected to have a vertical polarization component. By rotating the beam splitter (while maintaining the angular orientation towards the crystal) and taking measurements at approximately 0^o, 45^o, 90^o, 135^o (and 180^o, 270^o,315^o, 360^o), the polarization was to be detected. The spectrometer was connected via optic fiber to the telescopic tube.

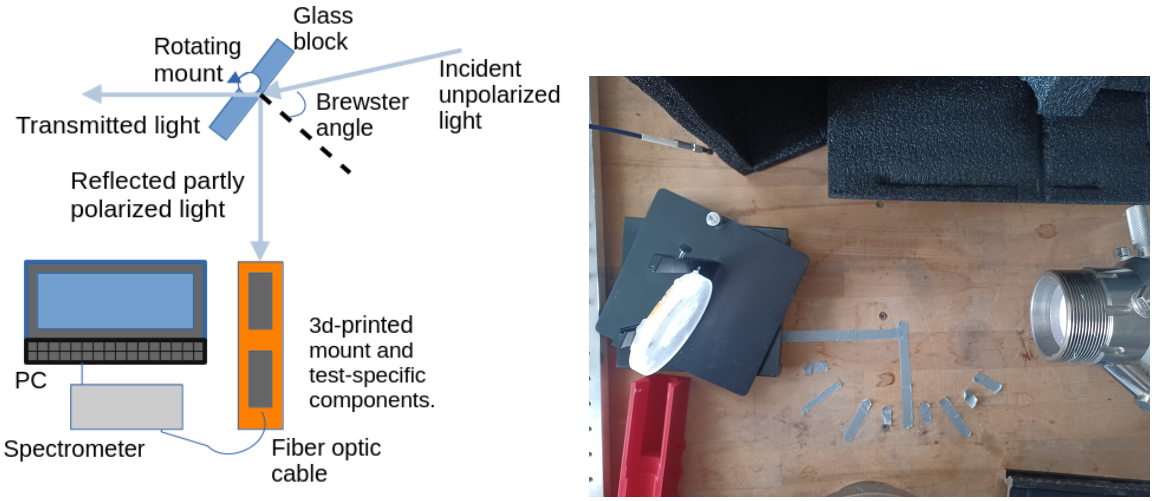

(a) Schematic of component tests. The rotating mount is in reality shaped as a hollow frame, allowing the incident light to pass through (unless reflected at the Brewster angle).

(b) Lab setup. The equipment to be tested is out of frame. To the right the opening of the Xenon lamp and the left, the quartz crystal.

Figure 7: Lab setup of component tests.

To prove a real polarization effect measurements were also taken for the same angular positions observing the xenon-lamp with the receiver directly. The integration time for the Brewster measurements and the reference measurements were 200 ms and 3 ms respectively.

Results: The direct spectra of the Xenon lamp can be seeen in figure 8. The direct light seems to be unpolarized because of the similarity of the spectra for different angles (given the nature of the source circularly polarized light seem an unlikely explanation). Something to note is that the spectra separated by 180^o are expected to be the exact same since the beam splitter fast axis goes completely through the components and so should measure the exact same thing twice per complete revolution. The full revolution is included for illustrative purposes. Figure 9 shows the spectra gathered of the light reflected from the crystal at the Brewster angle. That a polarization effect was achieved is evident, since the intensity drops markedly with the fast axis of the beam splitter deviating from the vertical orientation. At 45^o, 135^o, (as well as 225^o and 315^o) the spectra are at about half intensity, which is to be expected, since the component aligned with the beam splitter should be about half. That we do not have a perfect drop is probably due to the width of the beam and receiver aperture, causing a deviation from the Brewster orientation closer to the edges of the beam. Furthermore the surface of the crystal is not perfectly flat and there is probably also some back-scattering from the back-wall of the crystal. Some imperfections in the crystal was expected to cause an uneven refractive index throughout the block.

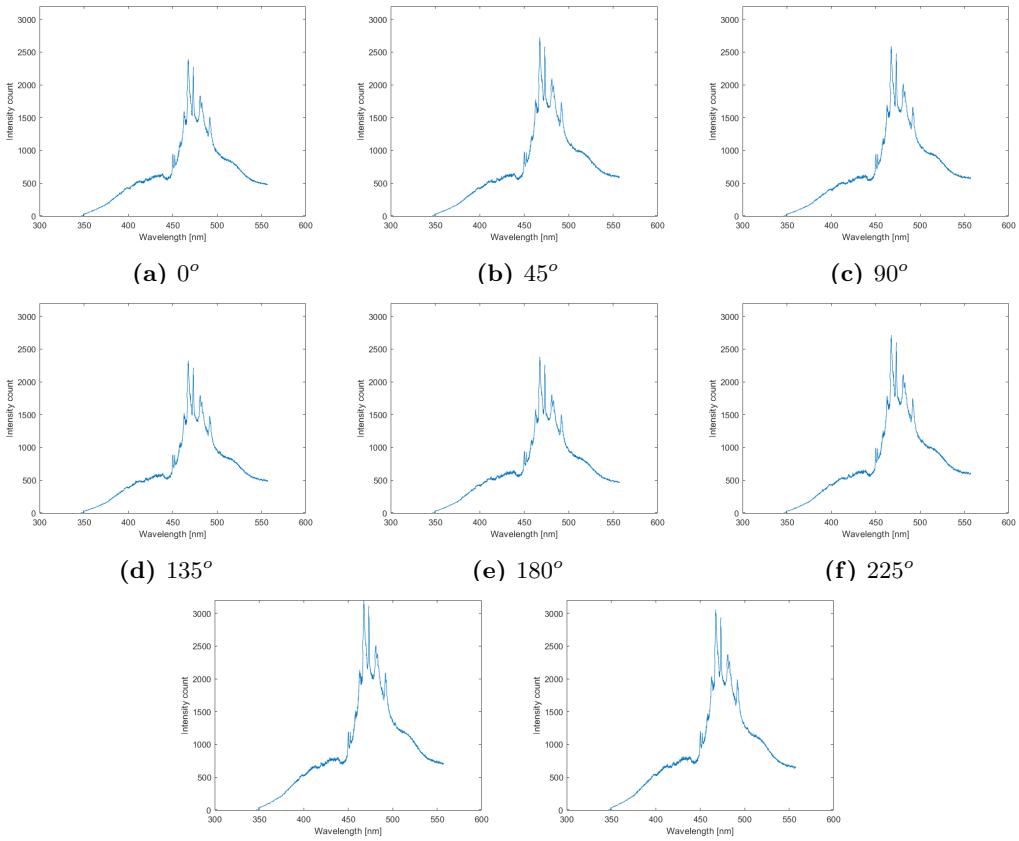

(a) 0^o **(b)** 45^o **(c)** 90^o

(d) 135^o **(e)** 180^o **(f)** 225^o

(g) 270^o **(h)** 315^o

Figure 8: Direct measurements of xenon-lamp to compare measurements with setup in Brewster angle (figure 9). Since the distribution and intensity are very similar between different orientations of the beam splitter, the signal is interpreted as being unpolarized.

3.3 Test of the Fresnel rhomb quarter wave retarder

Incident light with linear polarization angle deviating 45 degrees from the fast axis of the quarter wave retarder should be transformed into circularly polarized light by this component. According to Thorlabs, the Fresnel rhomb quarter wave retarder has a very even effect in the visible spectrum (it is achromatic). Therefore, it is expected that the spectra of the light passing through the rhomb is affected evenly [**20**].

Experiment: First, the beam splitter was mounted in front of the telescopic tube and the component placed in Brewster orientation. Next measurements were performed to verify that the light was polarized. Next the quarter wave Fresnel rhomb was placed between the quartz crystal and the beam splitter, oriented along the Brewster path with its fast axis rotated 45 degrees from the angle of polarization as measured in the previous step.

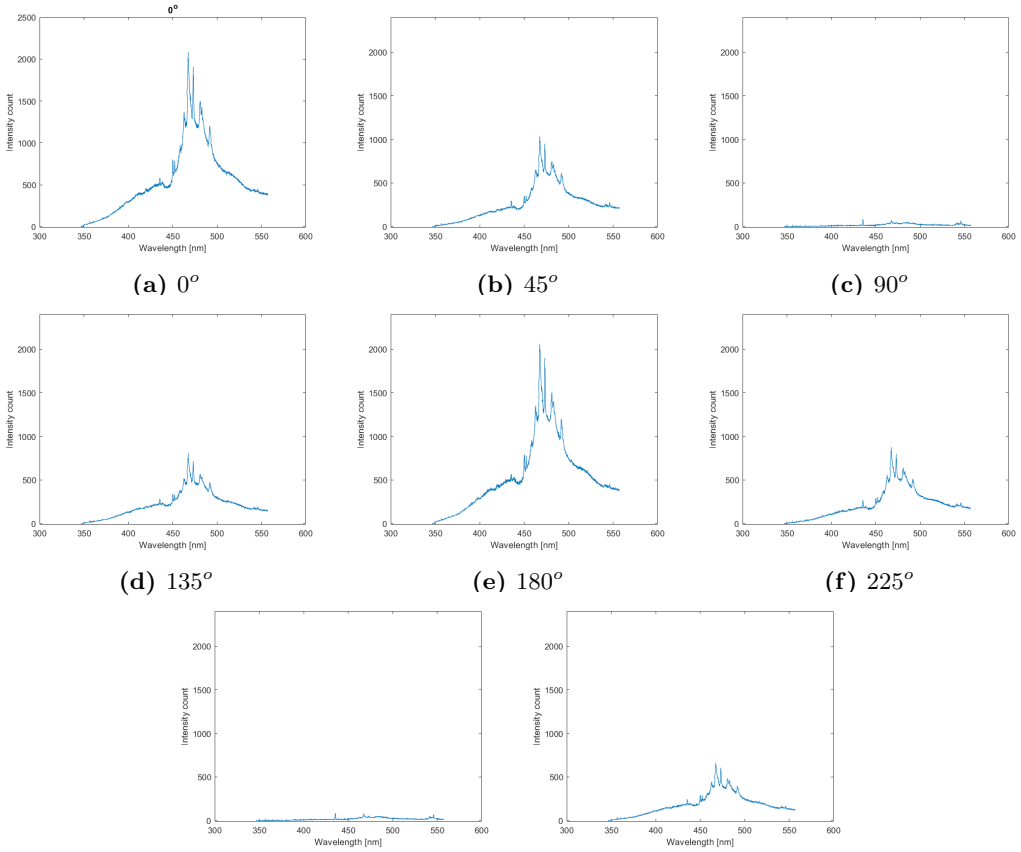

(a) 0^o **(b)** 45^o **(c)** 90^o

(d) 135^o **(e)** 180^o **(f)** 225^o

(g) 270^o **(h)** 315^o

Figure 9: Results of measurements using xenon-lamp and receiver in brewster angle configuration for different fast axis orientations. 0^o and 180^o indicate vertical orientation of the beam splitter fast axis. At 45^o and 135^o (or 225^o and 315^o) it is completely expected to find a 50 percent reduction for vertically polarized light.

Result: It turned out that the main axis of polarization was off the vertical axis by about 20^o clockwise for some reason (figure 10). Since the degree of polarization seemed similar to that of the polarization experiment above, this was accepted and the measurements of the quarter wave rhomb continued with the Fresnel rhomb fast axis rotated 45^o from the main polarization direction. Figure 11 show that the Fresnel rhomb had a clear circular polarizing effect.

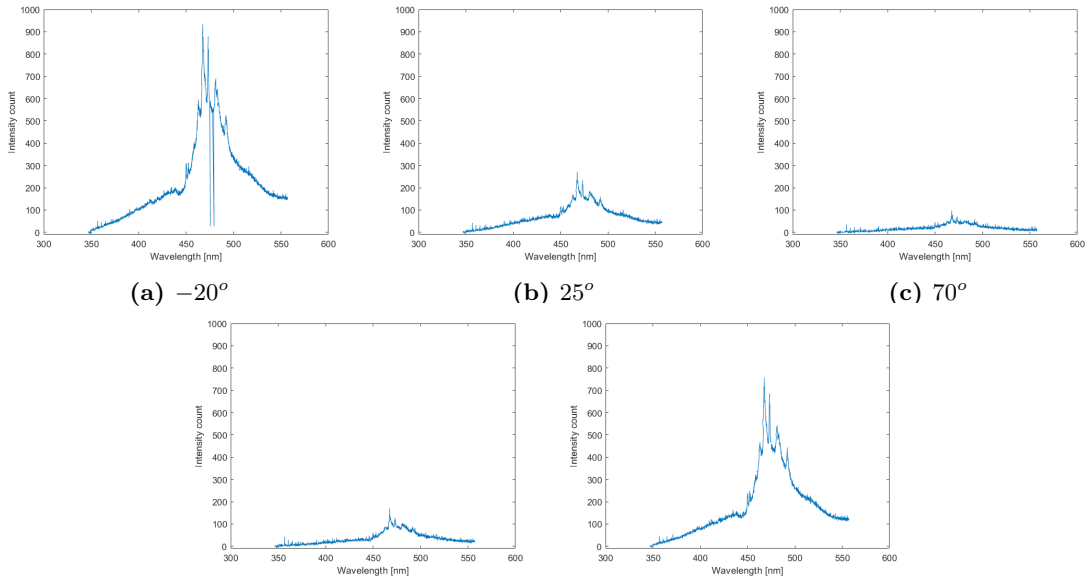

(a) -20^o **(b)** 25^o **(c)** 70^o

(d) 115^o **(e)** 160^o

Figure 10: Reference measurement in preparation of the quarter wave rhomb evaluation. The polarization was off vertical axis by approximately -20^o(that is clockwise).

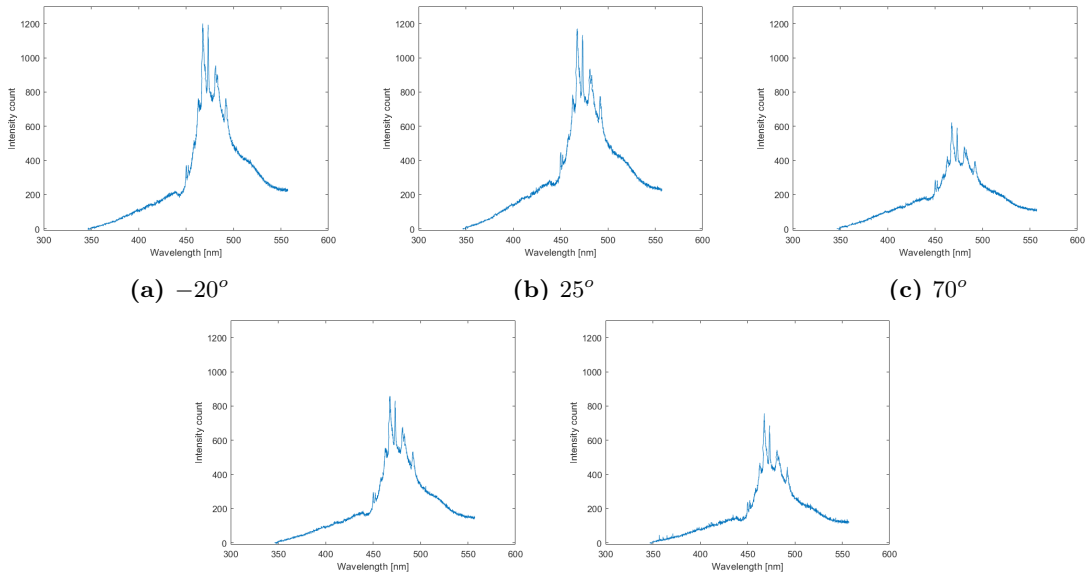

(a) -20^o **(b)** 25^o **(c)** 70^o

(d) 115^o **(e)** 160^o

Figure 11: Measurements with Fresnel rhomb in between quartz crystal and beam splitter, oriented along the Brewster angle and with fast axis oriented 45^o counter-clockwise from the measured main polarization direction of the incident light. A circularly polarizing effect is evident.

3.4 Test of the multiple order retarder

For the multiple order quarter wave retarder there may be a variation of the degree of circular polarization of the incident linearly polarized beam oriented towards 45 degrees of axis, for the lower end of the spectra due to the stated operating range of the component. The retardation distribution of the component has not been analyzed here.

Setup: The setup is similarly as before mounted in Brewster configuration. Before conducting these measurements, the main axis of polarization was first determined to -10^o. The multiple order retarder was mounted directly in front of the beam splitter with the fast axis oriented 45^o clockwise from the main axis of polarization. It was expected to find a circular polarizing effect in a cyclical wavelength-dependent manner (a modulation pattern).

Results: With an incoming signal similar to that seen in figure 8 or figure 10, it can be seen from figure 12 that the multiple order retarder have a circular polarizing effect in a wavelength dependent manner. The effect was not perfect, likely due to non-linearly polarized components of the reflected light and positional errors during measurements. An example would be an undetected deviation from the vertical orientation of the crystal. The area under the modulation pattern is presumably unpolarized light reflected from the quartz crystal (which would not have been visible with a good quality polarizing filter). Interestingly, the relative amplitude of the modulation pattern appears to be lower relative to the total intensity at 35^o degrees. The most likely cause is a relatively strong reflection of unpolarized light towards this angle because of some positional error.

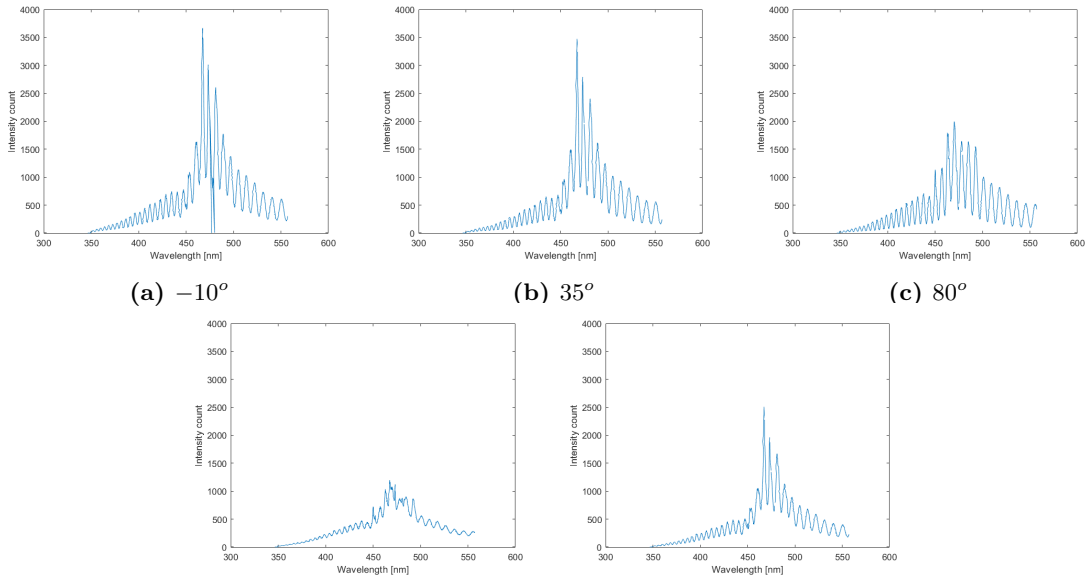

(a) -10^o **(b)** 35^o **(c)** 80^o

(d) 135^o **(e)** 170^o

Figure 12: Measurement results with the multiple order quarter wave retarder rotated 45^o from the main polarization direction of the light. The presence of a modulation pattern is indicative of some degree of polarization.

4 Lab tests part 2: system

The system tests involved both transmission tests similar to those described in the last section and tests on polarizing gas targets.

4.1 System transmission tests

Based on theory and the results of tests on the individual components, the combination should provide linearly polarized light when the fast axis of the components align with the angle of the incoming linearly polarized light. When the fast axis of the multiple order retarder from Halle (which is mounted between the Fresnel rhomb and the beam splitter) is rotated 45^o from the vertical, the main bulk of the light incident on the beam splitter should be circularly polarized.

Experiment: First the components are directionally placed along the Brewster direction, tightly mounted on the 3d-printed rack. The fast axis of both the Fresnel rhomb and the multiple order retarder were oriented vertically for the first test. For the second test the fast axis of the Fresnel rhomb was kept vertical and the fast axis of the multiple order retarder was rotated by 45^0 clockwise.

Results: The result of the first test can be seen in figure 13 which show a transmitted vertically polarized signal as expected. Interestingly a modulation pattern is visible in the spectra deviating from the main polarization direction but not in the vertical orientations. This is presumably because light incident with off-fast axis polarization will undergo elliptical polarization when passing through the polarimeter.

The result of second test can be seen in figure 14. Modulation patterns are present at 0^o, 90^o, 135^o (and 180^o). They are not present at 45^o. At 45^o the spectra seem to match what is underneath the modulation pattern of the other angles so it could be that what we see there is simply unpolarized light. Why we do not see a modulation pattern here is unclear.

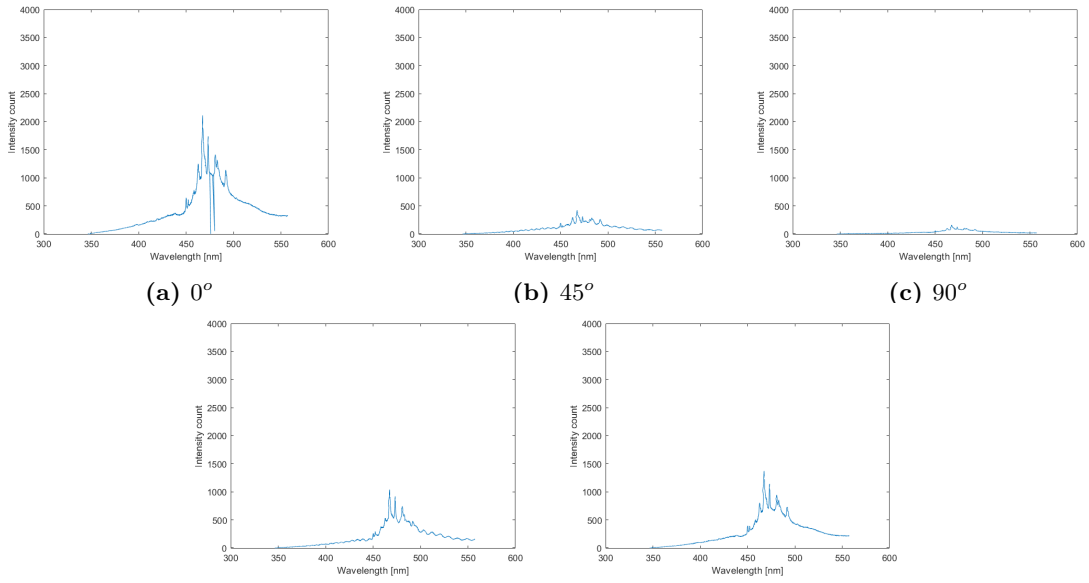

(a) 0^o **(b)** 45^o **(c)** 90^o

(d) 135^o **(e)** 180^o

Figure 13: Measurement results from the full system with both the Fresnel rhombs and the quarter wave multiple retarders fast axis oriented at 0^o. Non perfect but to some degree preserved polarization state from incident light.

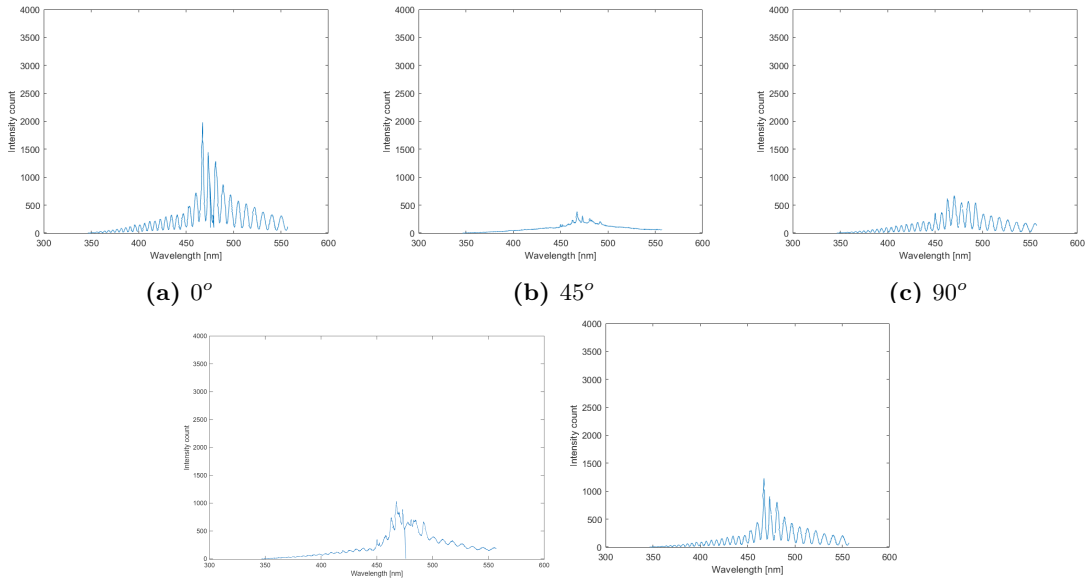

(a) 0^o **(b)** 45^o **(c)** 90^o

(d) 135^o **(e)** 180^o

Figure 14: Measurement results from the full system with the Fresnel rhomb fast axis oriented at 0^o and the multiple retarder fast axis oriented at 45^o. A circularly polarizing effect is evident.

4.2 Data processing method for retrieval of polarization curves

After extensive testing and working with the data, the method for polarization retrieval in figure 15 was established (Some example code available at `https://github.com/Polarimeter2025/ChanneledPolarimeterChalmers2025`, 2025). Towards the end of this project it was not yet completely stable for very noisy data which predominantly affected reliability of the lower end of the spectra. Therefore polarization curves are mainly retrieved from the upper half of the spectral interval. An illustration of this can be found by carefully studying figure 21 below, depicting results of a test on a target which will be described next.

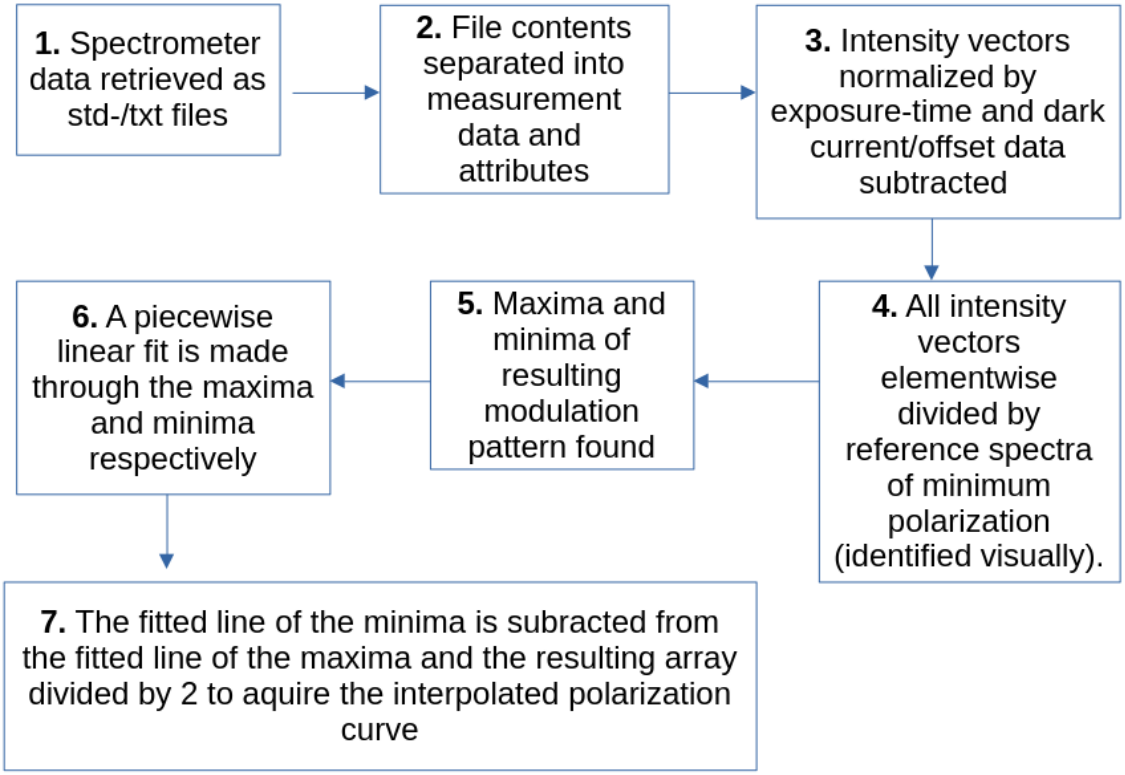

Figure 15: Overview of data processing method.

4.3 Polarizing smoke test

To test functionality and retrieval of polarization curves, a test was developed to mimic measurements that was later to be performed in the field.

4.3.1 Target substrate

Based on several studies ([**24**, **25**, **26**]), smoke from incense sticks or stearic candles were deemed a good proof-of-concept scattering substrate for laboratory testing, due to the average size of the particles, the proven polarizing effect and the practical convenience of its production. The polarization change in the lower end of the [350,550] nm interval should have a stronger Mie-scattered component than the higher end when observing light scattered on incense smoke. The aerosols created using incense seem to statistically be slightly too large to produce Rayleigh scattering in the range we are observing even if there could be outliers. To observe Rayleigh scattering at about 400 nm we need the particle to be about 40 nm, which is possible for particles in the lower end of the statistical size distribution according to literature. Smoke from stearic candles produces particles that are more suitable for detection of Rayleigh scattering but initial tests proved that the candles do not produce dense enough smoke to provide detectable scattering at all angles.

4.3.2 Setup

The setup is depicted in figure 16. Unpolarized light from a xenon-lamp enters a cylindrical glass container with incense smoke. The particles are in a state of slow flux and we want to prove that the system can find a signal above the noise in a stable manner. With the center of rotation in the middle of the container, measurements were taken at eleven even spaced angles in the 30-180 degree interval (0 being at the light source). The roof of the container was covered by tape, opaque to light from the surroundings. The wall of the container were adaptively covered by light blocking foam and fabric for different positions of the scattering angle detection. Thus, confounding radiation was minimized. For each measurement an associated dark current registration was saved. At each angle, direct detection with a telescopic tube, as well as an associated dark current measurement, were also taken. In this way a reference spectra at each angle was retrieved for comparison with the spectra retrieved by the polarimeter. The exposure time was adapted manually at each angle to avoid saturation while still capturing enough photons to produce a good enough signal to noise ratio. It was expected that the wall of the glass container would not change the polarization state of the scattered light significantly because of the normal incidence angle.

4.3.3 Results

Figure 17a shows the shape of the intensity spectra gathered directly at different scattering angles, normalized independently for each angle. The sinusoidal variation of the curve in figure 17b demonstrates the polarization component of the signal detected with the full instrument. The amplitude of the oscillations maps the degree of polarization.

Figure 18 displays the fractional difference between direct measurements and polarimetric measurements. Figure 19 displays the results of applying the method of figure 15 to the retrieved data. The shape of the polarization diagrams is what would be expected for Rayleigh-scattering with a maximum at 90 degrees [**26**] but also for Mie -scattering on spherical particles [**27**]. Given the

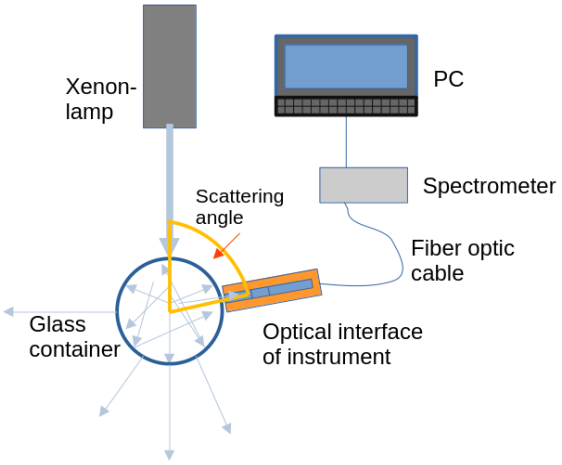

(a) Schematic of lab set up. Note that the optical interface sitting on the yellow rack was manually rotated between measurements to aquire data for different scattering angles. The center of rotation was at the center of the container.

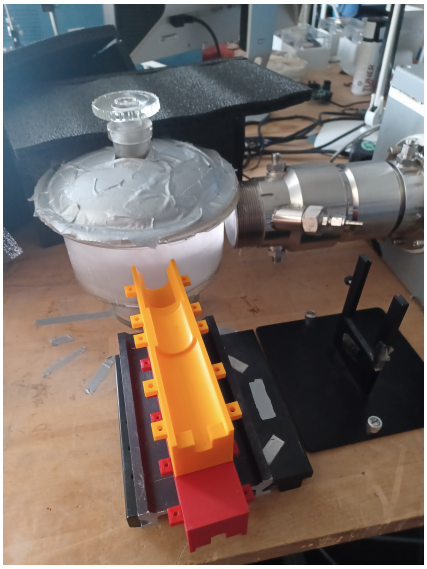

(b) Component mount (yellow) and container with smoke, illuminated by the Xenon-lamp. In this image the polarimeter is not mounted. When experiments were performed, the container was almost completely shielded from light, apart from the Xenon-lamp.

Figure 16: Images depicting the experiment of analyzing the polarizing effect incense smoke.

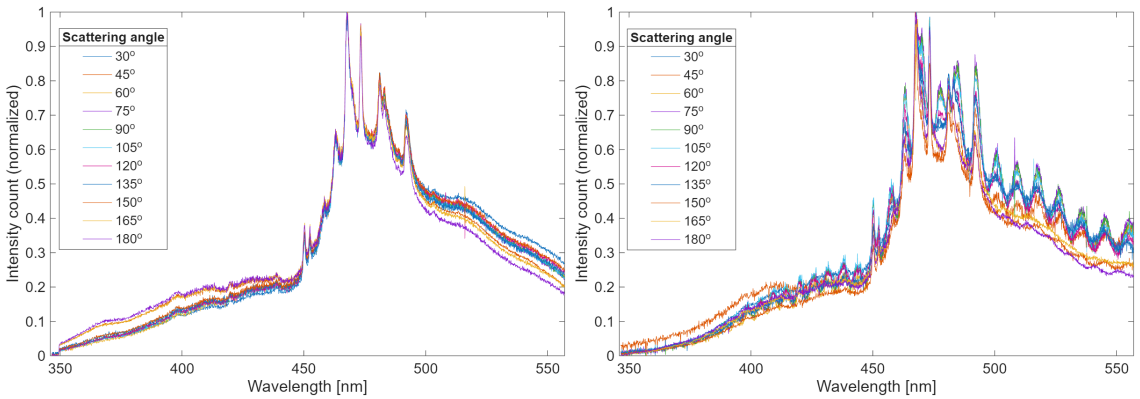

(a) Direct measurement of scattered light from the container, using only the telescopic tube.

(b) Measurements using the full polarimeter. The oscillations are indicative of a polarized signal.

Figure 17: Measurement if scattered light from the container, using the full polarimeter.

expected average size of the particles it is somewhat more likely that the polarization is caused by Mie-scattering. The most important conclusion is that the polarimeter and data processing method is capable of retrieving accurate polarization diagrams.

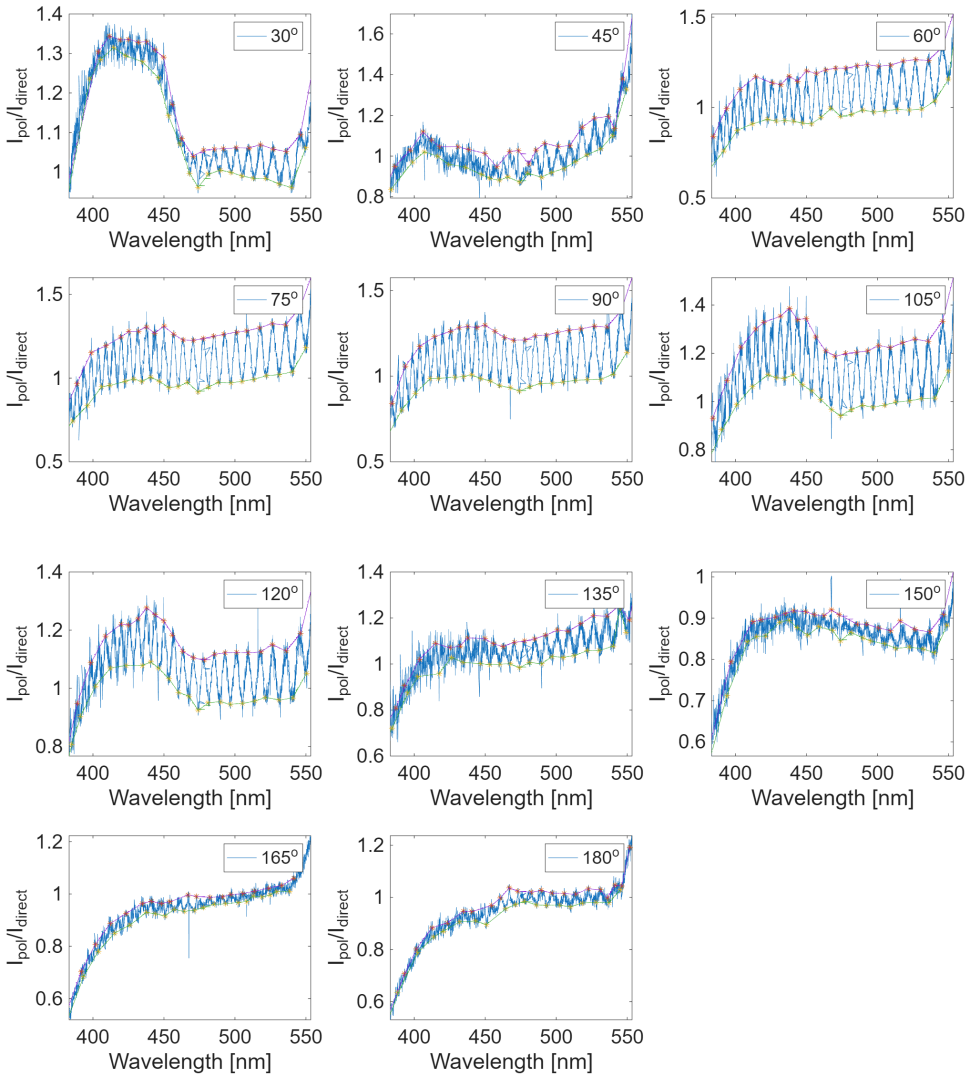

Figure 18: Intensity of light scattered by the incense smoke. The intensity of the polarimeter measurements divided by the direct measurements per scattering angle. Also on display the maxima- and minima-fitted curves. These graphs illustrates step 4-6 of the data processing method from figure 15.

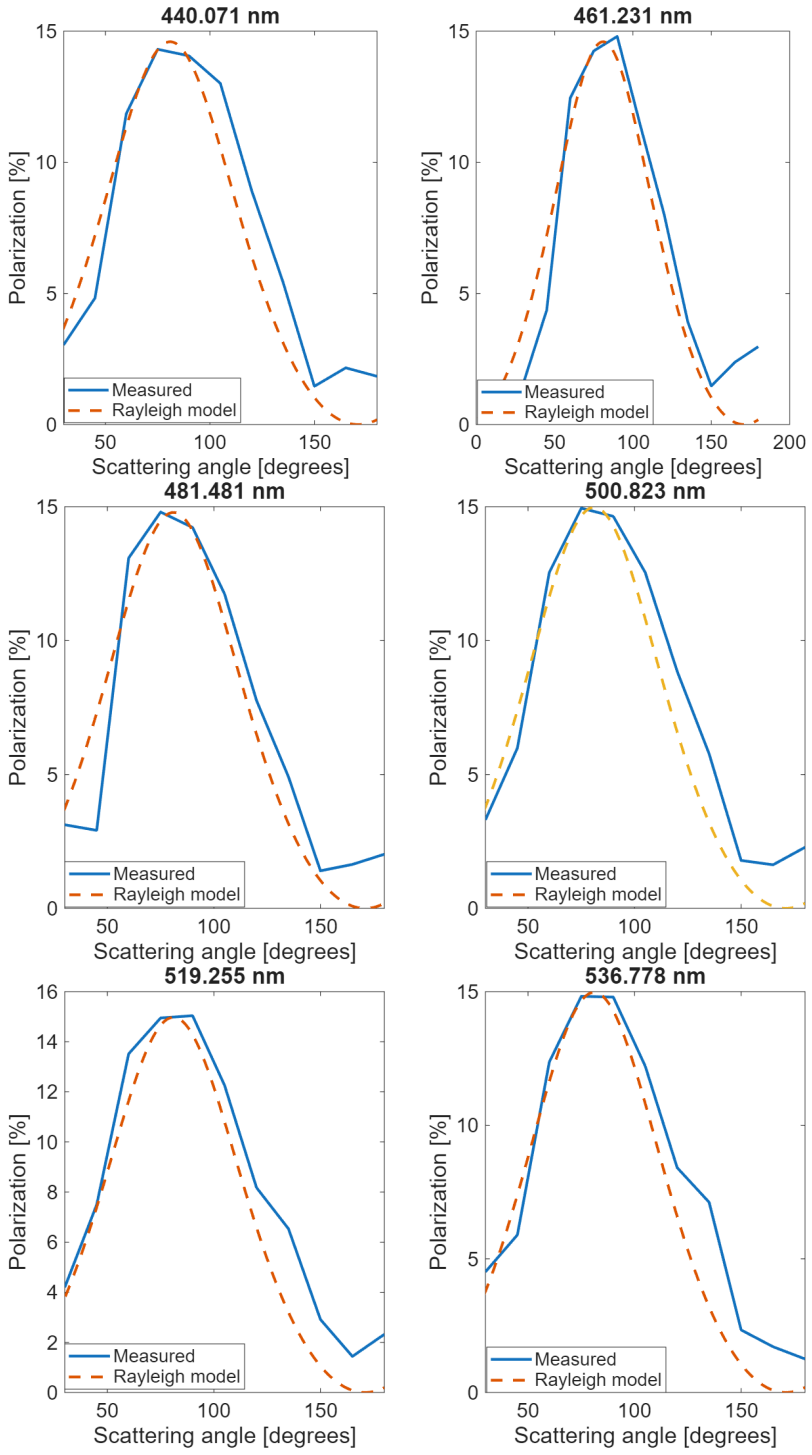

Figure 19: Polarization diagrams displaying the polarizing effect of the incense smoke.

5 Incorporation into Novac-equipment

It was decided that the optimal way to perform a large number of precise angle measurements was to incorporate the polarimeter into existing NOVAC observation equipment; such "DOAS-units" were readily available in the lab at Chalmers. The process will be described in this section.

5.1 Hardware

Figure 20 shows the outline of the NOVAC-unit with the final placement of the polarimeter. At first the design of the polarimeter casing put the polarimeter on the outside of the unit but once the casing had been designed, printed and mounted, it was found that the motor was not strong enough to move the polarimeter. The choice was therefore made to place the polarimeter after the mirror, along the unit axis. In this way the polarimeter does not move with the mirror, thus not putting any load on the motor. The final design of the polarimeter casing can be seen in figure 21 and the printed casing with components can be seen in figure 22.

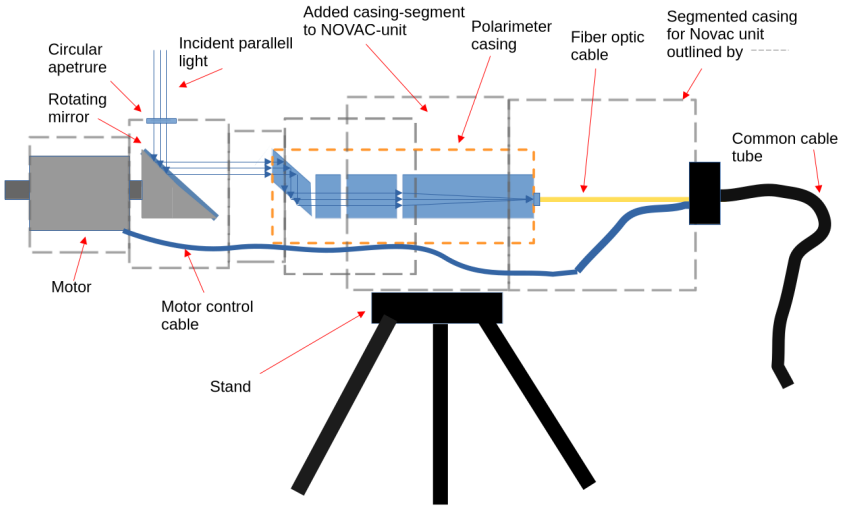

Figure 20: Schematic of Novac unit with inserted polarimeter.

The unit functions such that the motor rotates the mirror which has a fixed position relative to the circular aperture in the casing, meaning that the aperture follows the movement of the mirror. The mirror is oriented at a 45^o angle relative to both the aperture and the polarimeter, so the angle of incidence and reflection remains the same throughout the mirror rotation. What do change throughout the rotation is the angle of polarization of the light incident on the polarimeter, relative to its aperture to the Fresnel rhomb. The full details of the NOVAC-unit and the mounted polarimeter can be seen in figure 23. The only modification to the NOVAC-unit apart from the polarimeter was the addition of a casing segment so the polarimeter would fit lengthwise. The motor is controlled via a script that is run on a computer connected via cable.

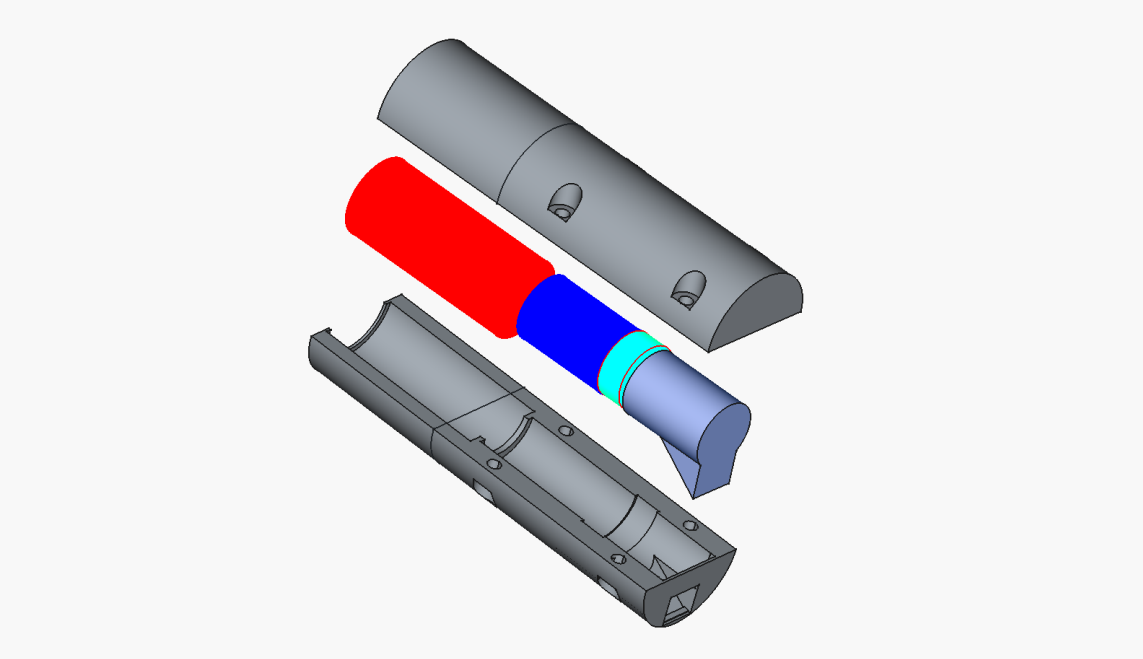

Figure 21: CAD schematics of polarimeter casing. An approximate polarimeter schematic is also included for visualization. Red: telescopic tube, blue: beam splitter, teal: multiple order retarder, metallic blue: quarter wave retarder.

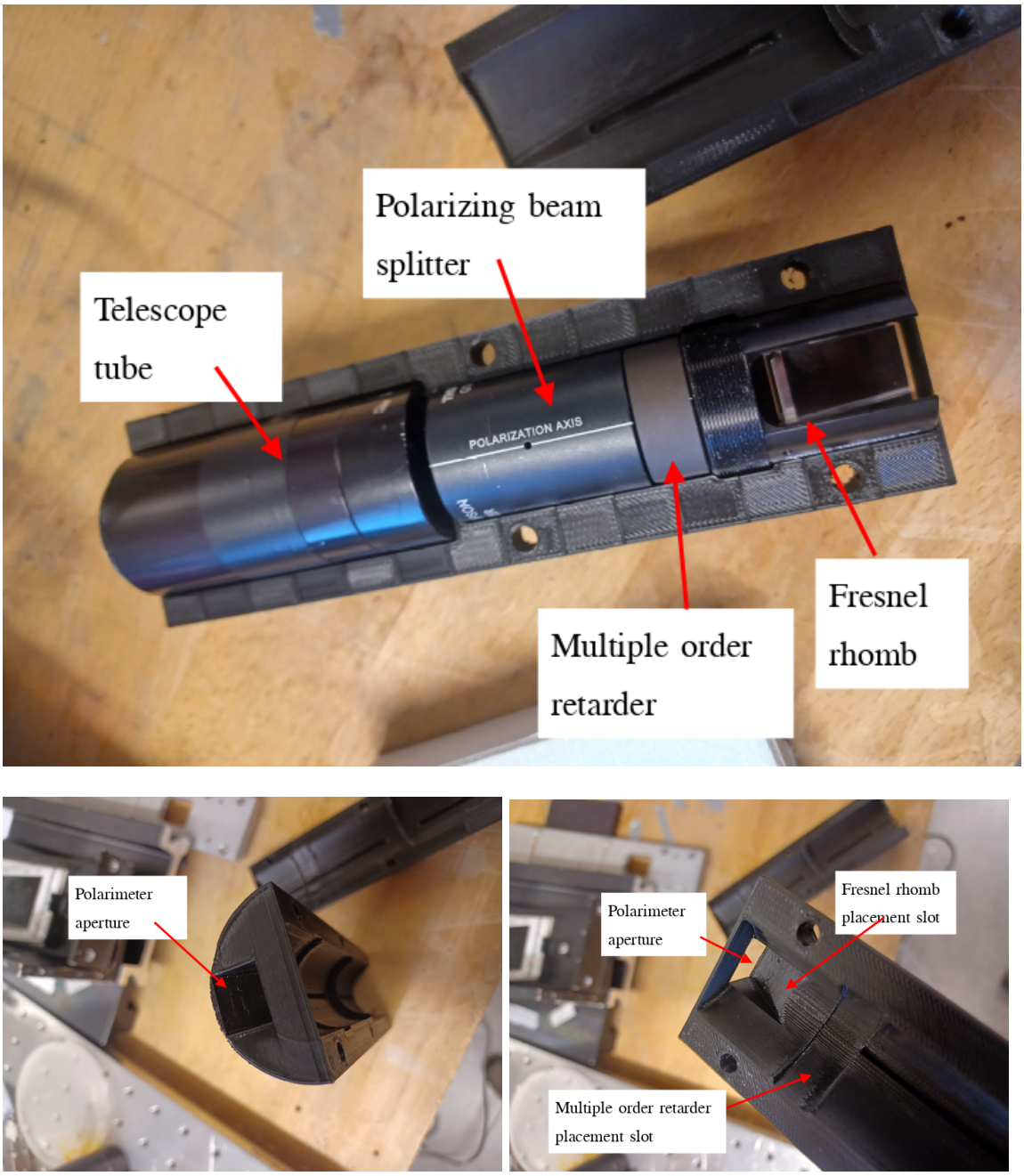

Figure 22: Top: Polarimeter in 3d-printed casing. **Bottom left:** front view of the polarimeter aperture, the other half of the casing can be seen in the background. **Bottom right:** inside view of the polarimeter aperture and how the Fresnel rhomb can be fitted against it.

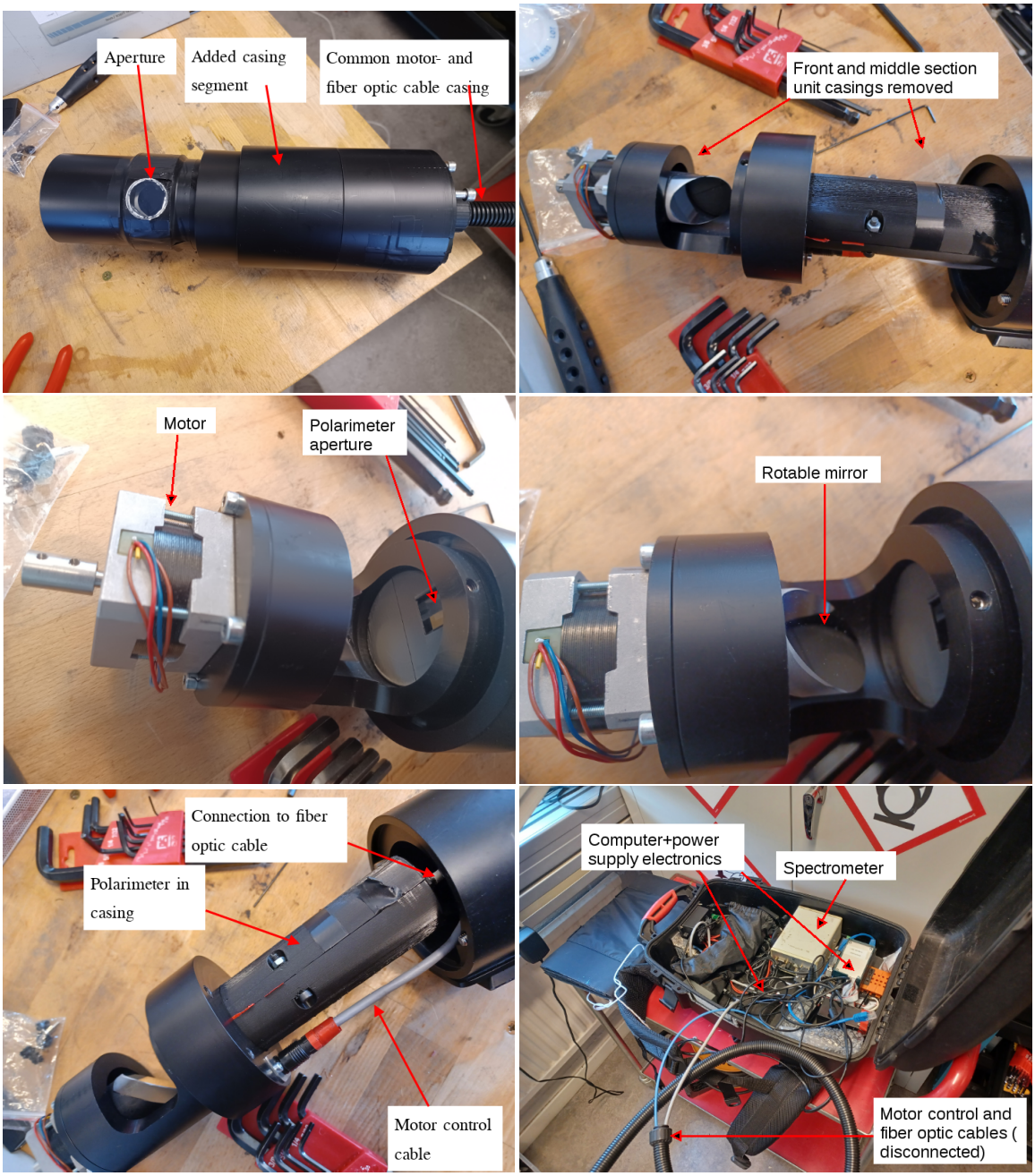

Figure 23: Photos of how the polarimeter is incorporated into existing NOVAC-equipment.

5.2 Influence of the rotating mirror on measurements

As the mirror rotates through measurement series, the light reflected on the mirror will reach the polarimeter aperture at different orientations polarization-wise. The mirror is made of aluminum and the equations that produce elements of the Mueller matrix for the reflection has been solved numerically for illustrative purposes at about 620nm. At the incidence angle of 45^o, the phase shift between s-polarized and p-polarized light is approximately at -13^o, using an extinction factor of 3.63 and an index of refraction of 1.44 (45^o) for aluminum [**28**]. The reflectivity for s- and p-polarized light at 45^o incidence angle was calculated using the same source to 0.935 and 0.875 respectively and the Mueller matrix of the mirror at this incidence angle is [**16 (p.105)**]:

$$M(620\text{nm})_{\text{mirror}} = \begin{bmatrix} 0.82 & 0.11 & 0 & 0 \\ 0.11 & 0.82 & 0 & 0 \\ 0 & 0 & -0.8 & 0.18 \\ 0 & 0 & -0.18 & -0.8 \end{bmatrix}, M(\lambda)_{\text{mirror}} = \begin{bmatrix} m_{11} & m_{12} & 0 & 0 \\ m_{21} & m_{22} & 0 & 0 \\ 0 & 0 & m_{33} & m_{34} \\ 0 & 0 & m_{43} & m_{44} \end{bmatrix} \tag{21}$$

To be sure of the reflectivity of the mirror it would have to be measured but the values from literature were at least realistic. Multiplying the matrix above with the transformation matrix (equation 12) produce the mounted transformation matrix:

$$M_{\text{MOR}} M_{\text{FR}} M_{\text{mirror}} =$$

$$= \begin{bmatrix} m_{11} & m_{12} & 0 & 0 \\ m_{21}\cos(2\pi\delta/\lambda) & m_{22}\cos(2\pi\delta/\lambda) & -m_{33}\sin(2\pi\delta/\lambda) & -m_{34}\sin(2\pi\delta/\lambda) \\ 0 & 0 & -m_{43} & -m_{44} \\ m_{21}\sin(2\pi\delta/\lambda) & m_{22}\sin(2\pi\delta/\lambda) & m_{33}\cos(2\pi\delta/\lambda) & m_{34}\cos(2\pi\delta/\lambda) \end{bmatrix} = M_{\text{T2}} \tag{22}$$

The new output signal (before the beam splitter) becomes:

$$M_{\text{T2}} S = \begin{bmatrix} m_{11}S_0 + m_{12}S_1 \\ m_{21}\sin(2\pi\delta/\lambda)S_0 + m_{22}\cos(2\pi\delta/\lambda)S_1 - m_{33}\sin(2\pi\delta/\lambda)S_2 - m_{34}\sin(2\pi\delta/\lambda)S_3 \\ -m_{43}S_2 + m_{44}S_3 \\ m_{21}\sin(2\pi\delta/\lambda)S_0 + m_{22}\sin(2\pi\delta/\lambda)S_1 + m_{33}\cos(2\pi\delta/\lambda)S_2 + m_{34}\cos(2\pi\delta/\lambda)S_3 \end{bmatrix} \tag{23}$$

A new representation of polarization states, before the light enters the beam splitter, are represented in table 4. Transformations of arbitrary elliptically and linearly polarized light were omitted for room, to make it easier to interpret. In short the effect of the mirror is an elliptical polarization. It seems that in relation to the purpose of the instrument, the transformation is similar as before, however, it seems that the horizontal and vertical light components might become scaled differently by some percentage points, depending on the polarization angle of the incident beam. Some minor distorsion might occur for different polarization states. Notably, unpolarized light seem to undergo some slight degree of polarization.

Table 4: Mathematical representation of polarizers effect on the polarization of the passing light using the updated transformation matrix, before it enters the beamsplitter.

Polarization of incident light	**Stokes vector of incident light**	**Stokes vector of transmitted light**	**Polarization of transmitted light**
Linear vertical	$\begin{bmatrix} 1 \\ -1 \\ 0 \\ 0 \end{bmatrix}$	$\begin{bmatrix} m_{11} - m_{12} \\ m_{21}\sin(2\pi\delta/\lambda) - m_{22}\cos(2\pi\delta/\lambda) \\ 0 \\ m_{21}\sin(2\pi\delta/\lambda) - m_{22}\sin(2\pi\delta/\lambda) \end{bmatrix}$	Elliptical dependent on m_{xx}
Linear horizontal	$\begin{bmatrix} 1 \\ 1 \\ 0 \\ 0 \end{bmatrix}$	$\begin{bmatrix} m_{11} + m_{12} \\ m_{21}\sin(2\pi\delta/\lambda) + m_{22}\cos(2\pi\delta/\lambda) \\ 0 \\ m_{21}\sin(2\pi\delta/\lambda) + m_{22}\sin(2\pi\delta/\lambda) \end{bmatrix}$	Elliptical dependent on m_{xx}
Linear 45^o	$\begin{bmatrix} 1 \\ 0 \\ 1 \\ 0 \end{bmatrix}$	$\begin{bmatrix} m_{11} \\ (m_{21} - m_{33})\sin(2\pi\delta/\lambda) \\ -m_{43} \\ m_{21}\sin(2\pi\delta/\lambda) + m_{33}\cos(2\pi\delta/\lambda) \end{bmatrix}$	Elliptical dependent on m_{xx}
Left circular	$\begin{bmatrix} 1 \\ 0 \\ 0 \\ -1 \end{bmatrix}$	$\begin{bmatrix} m_{11} \\ (m_{21} + m_{34})\sin(2\pi\delta/\lambda) \\ -m_{44} \\ m_{21}\sin(2\pi\delta/\lambda) - m_{34}\cos(2\pi\delta/\lambda) \end{bmatrix}$	Elliptical dependent on m_{xx}
Right circular	$\begin{bmatrix} 1 \\ 0 \\ 0 \\ 1 \end{bmatrix}$	$\begin{bmatrix} m_{11} \\ (m_{21} - m_{34})\sin(2\pi\delta/\lambda) \\ m_{44} \\ m_{21}\sin(2\pi\delta/\lambda) + m_{34}cos(2\pi\delta/\lambda) \end{bmatrix}$	Elliptical dependent on m_{xx}
Unpolarized	$\begin{bmatrix} 1 \\ 0 \\ 0 \\ 0 \end{bmatrix}$	$\begin{bmatrix} m_{11} \\ m_{21}\sin(2\pi\delta/\lambda) \\ 0 \\ m_{21}\sin(2\pi\delta/\lambda) \end{bmatrix}$	Cyclical partial polarization

The final Stokes vector after the beam splitter is:

$$S_{\text{out}} = M_{\text{BS}} M_{\text{T2}} S =$$

$$= \frac{1}{2}\begin{bmatrix} (m_{11} + m_{12}\sin(2\pi\delta/\lambda))S_0 + (m_{21} + m_{22}\cos(2\pi\delta/\lambda))S_1 - m_{33}\sin(2\pi\delta/\lambda)S_2 - m_{34}\sin(2\pi\delta/\lambda)S_3 \\ (m_{11} + m_{12}\sin(2\pi\delta/\lambda))S_0 + (m_{21} + m_{22}\cos(2\pi\delta/\lambda))S_1 - m_{33}\sin(2\pi\delta/\lambda)S_2 - m_{34}\sin(2\pi\delta/\lambda)S_3 \\ 0 \\ 0 \end{bmatrix} \tag{24}$$

This means that the original equation used for the SPEX-instruments (equation 16) is no longer completely valid for this system. What follows is a derivation of a modified equation. Note that it is only valid for the vertical transformation of the output, S_v ; the horizontal output have some different signs since the beam splitter -mueller matrix have some different signs for that signal. The derivation start at the point of equating the output with the Stokes transformation:

$$S_v = S_{\text{out}}(1,1) = \frac{1}{2}(((m_{11} + m_{12}\sin(2\pi\delta/\lambda))S_0 + (m_{21} + m_{22}\cos(2\pi\delta/\lambda))S_1 -$$

$$-m_{33}\sin(2\pi\delta/\lambda)S_2 - m_{34}\sin(2\pi\delta/\lambda)S_3 =$$

$$= \frac{1}{2}(\overbrace{(m_{11} + m_{12}\sin(2\pi\delta/\lambda))S_0 + (m_{21} + (m_{22} - m_{33})\cos(2\pi\delta/\lambda))S_1 - m_{34}\sin(2\pi\delta/\lambda)S_3}^{A(\lambda,\delta,m_{11},m_{12},m_{21},m_{22},m_{33},m_{34})} + \tag{25}$$

$$+m_{33}(\cos(2\pi\delta/\lambda)S_1 + \sin(2\pi\delta/\lambda)S_2)) =$$

$$= \frac{1}{2}(A + m_{33}S_0(\pm\overbrace{\frac{\sqrt{S_1^2 + S_2^2}}{S_0}\cos(2\pi\delta/\lambda - \arctan(S_2/S_1))}^{\text{through trigonometric rule}})$$

Per definition, the degree of linear polarization and the angle of polarization is given from elements of the Stokes vector by:

$$P = \frac{\sqrt{S_1^2 + S_2^2}}{S_0}\,,\ \textit{Degree of linear polarization.}$$

$$\omega = \frac{1}{2}\arctan(S_2/S_1)\,,\ \textit{Angle of polarization.} \tag{26}$$

Now the expression in equation 25 can be written as:

$$S_v = \frac{1}{2}(A \pm m_{33}S_0P\cos(\overbrace{2\pi\delta/\lambda - 2\omega}^{\phi})) = \frac{1}{2}(S_0(A/S_0 \pm m_{33}P\cos(\phi))) =$$

$$= \frac{S_0}{2}(m_{11} + m_{12}\sin(2\pi\delta/\lambda))+$$

$$+(m_{21} + (m_{22} - m_{33})\cos(2\pi\delta/\lambda))\frac{S_1}{S_0} - m_{34}\sin(2\pi\delta/\lambda)\frac{S_3}{S_0} \pm m_{33}P\cos(\phi)) = \tag{27}$$

$$= \frac{S_0m_{33}}{2}\left(\frac{m_{11}}{m_{33}} + \frac{m_{12}}{m_{33}}\sin(2\pi\delta/\lambda)+\right.$$

$$\left.+\left(\frac{m_{21}}{m_{33}} + \frac{m_{22} - m_{33}}{m_{33}}\cos(2\pi\delta/\lambda)\right)\frac{S_1}{S_0} - \frac{m_{34}}{m_{33}}\sin(2\pi\delta/\lambda)\frac{S_3}{S_0} \pm P\cos(\phi)\right)$$

This is the final output signal that is measured. Or, in terms of the input intensity I_a:

$$\boxed{\begin{aligned} I = I_aS_v = \frac{I_am_{33}}{2}\left(\frac{m_{11}}{m_{33}} + \frac{m_{12}}{m_{33}}\sin(2\pi\delta/\lambda))+\right. \\ \left.+\left(\frac{m_{21}}{m_{33}} + \frac{m_{22} - m_{33}}{m_{33}}\cos(2\pi\delta/\lambda)\right)\frac{S_1}{S_0} - \frac{m_{34}}{m_{33}}\sin(2\pi\delta/\lambda)\frac{S_3}{S_0} \pm P\cos(\phi)\right) = \\ = \frac{I_am_{33}}{2}(A(\lambda, \delta, m_{11}, m_{12}, m_{21}, m_{22}, m_{33}, m_{34}) \pm P\cos(\phi)) \end{aligned}} \tag{28}$$

The S1- and S3- associated terms will, in general, probably be significantly smaller than the first terms and the last polarization-term. For 620nm, as an example, the equation above should be reducible to:

$$\boxed{I = \frac{I_a}{2}(1.02 + 0.14\sin(2\pi\delta/\lambda)) \pm P\cos(\phi))} \tag{29}$$

That the first term in the parentheses, "1.02", is larger than 1 is presumably offset by the terms in this equation but also the horizontal component.

The effect of the mirror across the spectra can be resolved numerically and then partly offset from the results, as a component of the data processing algorithm (figure 15). That the offset is accurate should then be verified experimentally. This has not been done in the scope of this project.

A notable change is that light which is incident with circular polarization will now not be completely evenly dispersed between vertical and horizontal orientations of the beam splitter, this should

influence the modulation pattern to some degree. It could also influence the measured degree of linear polarization, but since circular polarization is so uncommon, the effect is expected to be negligible. Next, an experiment that was performed to evaluate if the mirror can catch a good enough signal for different orientations is presented.

5.2.1 Setup

The experimental setup is depicted in figure 24. Note that the angle of incidence of the light source on the mirror does not change throughout the measurement. The polarimeter is rotated manually relative to the mirror. The relative motion between the mirror and the polarimeter is the same as it would be for a motorized field test but since the light source is fixed relative to the mirror the only thing that should shift is the angle of polarization relative to the polarimeter aperture, throughout the measurement. Since we pass the unpolarized light through a vertical polarization filter, the light incident on the mirror is polarized parallel to the surface in the vertical direction. This means that the reflected light will also be mainly vertically polarized.

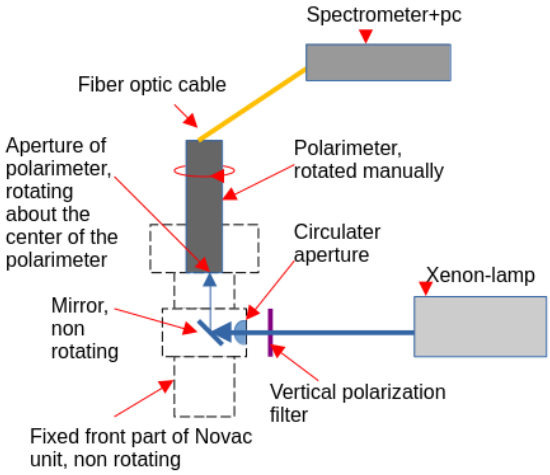

(a) Schematic of experiment.

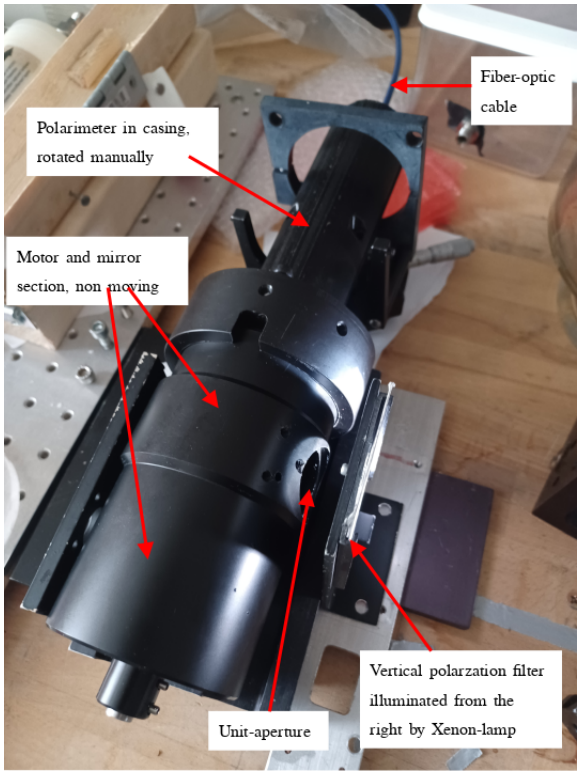

(b) Photo of the setup. The white frame contains the polarization filter.

Figure 24: Images of the experiment to test the influence of the mirror on the measurements. The instrument frame was rotated manually to gather data for different incidence angles.

5.2.2 Results

The results are summarized in figure 25. The different incidence angles seem to cause a phase shift of the signal. Note that this is directly translated as a changing angle of polarization. Furthermore, the decreasing amplitude in relation to rotation of the polarimeter is likely due to the fact that less light is reflected back to the polarimeter at the extreme angles. The fraction lost due to non perfect reflectivity of the mirror should be visible already in the horizontal position of the instrument. A fraction is also lost because of the polarization filter. The polarization signal remains pure and almost completely undistorted throughout the rotation though and this is what is most important since the degree of polarization is the main interest, not the angle. The decreasing intensity for odd angles is expected to not distort later measurements since it is expected to affect unpolarized light an equal amount.

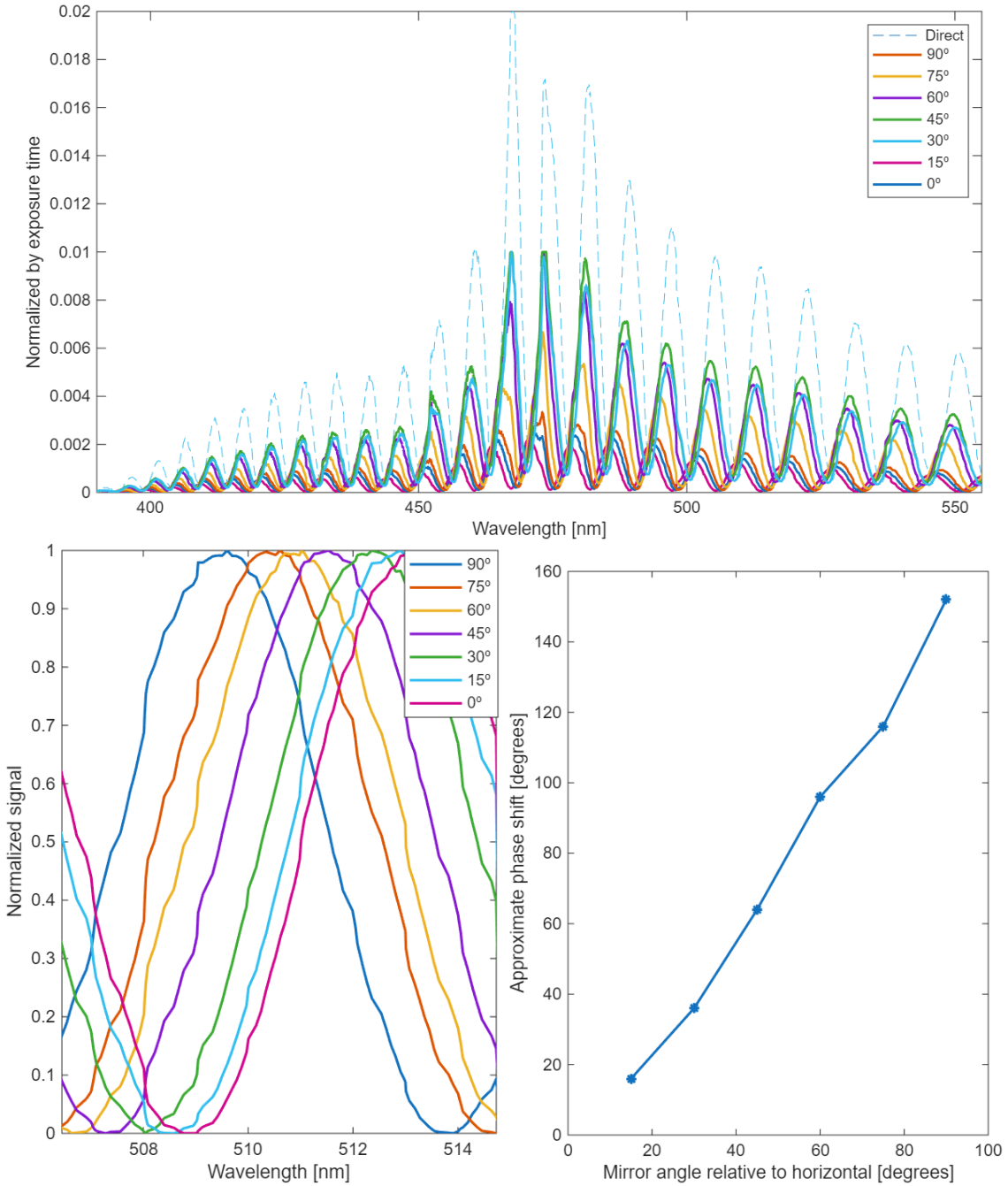

Figure 25: Effect on signal by aperture mirror. **Top:** The varying intensity comes from the fact that less light reaches the mirror at odd angles. The elevated baseline of some angles could be due to different exposure time but its origin have not been investigated in detail. **Bottom left:** A segment of the spectra with the curves normalized to make the phase difference more apparent. **Bottom right:** The phase delay range from 15^o to 155^o.

6 Field tests

The goal of the field tests was to verify the prototype's intended functionality. The most basic test of functionality was the principal plane measurements. After these, measurements on a smoke plume were performed.

For most of the principle plane measurements, the exposure time was estimated from a fraction of the longest possible exposure time and kept constant throughout the measurement cycle. A few different fractions was attempted between 40% and 70%. For the most part these produce good retrievals for directions off-sun, but the close-to-sun and sun measurements invariably became saturated. Therefore an approach of adaptive exposure time at each angle was later implemented for a few of the principle plane tests and the smoke plume tests. This made the measurements take longer time than before but provided non-saturated spectra at each angle.

6.1 Principle plane measurements

The measurements were taken at Chalmers in 30-60 minute sessions on days with no precipitation and mostly clear skies. The reason for the limited time duration was the ideal positioning of the sun between buildings for this time, which allowed for wide angle measurements, while having access to power. Since good measurements could be retrieved in this way, time and money was not spent on transporting the equipment to a field for these measurements.

6.1.1 Method

Integration-time was set to gather light until 40, 50, and 75 percent of maximum exposure time. It was constant for each instrument rotation. The range of measurement was 3.6*49=176 degrees with a starting elevation of 0 degrees. Three measurements series were taken for each percentage of saturation to compensate for variation due to passing clouds in some cases. Figure 26 shows an illustration of the measurement environment. A few measurement series were also taken at a 90^o azimuth difference to the principal plane. The geometry is displayed schematically in figure 27.

6.1.2 Results

Figure 28 shows the results of the principle plane measurements for a few selected wavelengths (same as for the incense smoke test). The peaks and noise in the central dip where minimum polarization is expected could be due to the sun being a few degrees off the principal plane in the southward azimuth direction. Apart from that the graphs show what is to be expected [**29**].

Figure 29 show the results of the measurements with the retrieval plane rotated 90^o from the sun in the azimuth direction. It was expected to see a double hump in the polarization diagram since the instrument rotation would approach and leave an orientation of light retrieval from a scattering angle of 90^o twice during the rotation. Note that it is yet unclear to what degree the elliptically polarizing effect of the rotating mirror, contribute to the polarization baseline for all measurements.

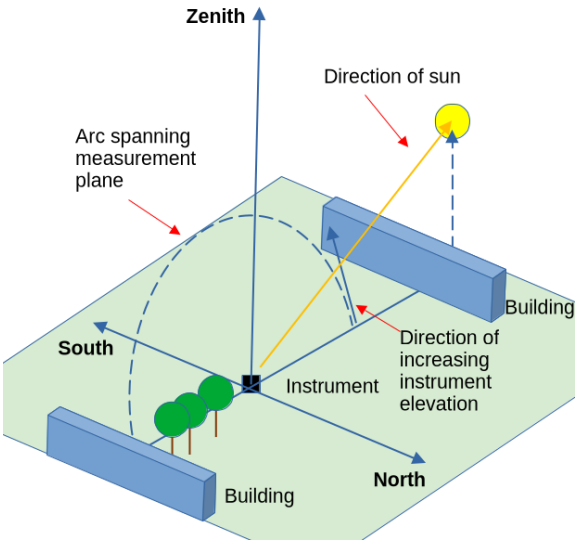

Figure 26: Schematic overview of principal plane measurement environment.

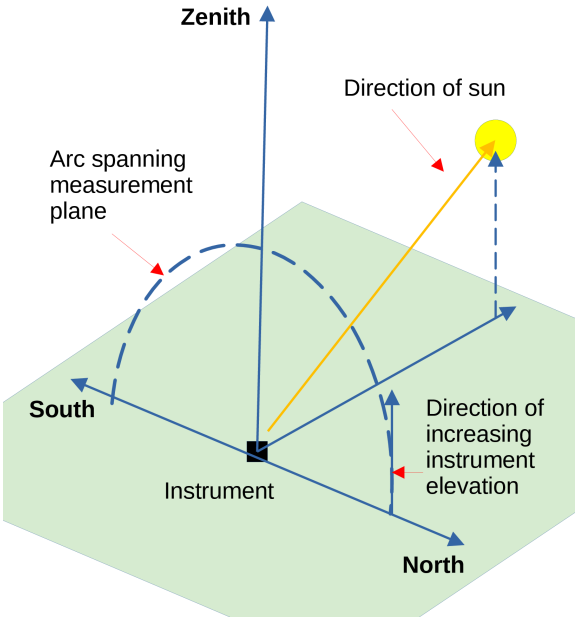

Figure 27: Geometry of measurement with a 90^o azimuth deviation between the direction of the Sun and the measurement plane.

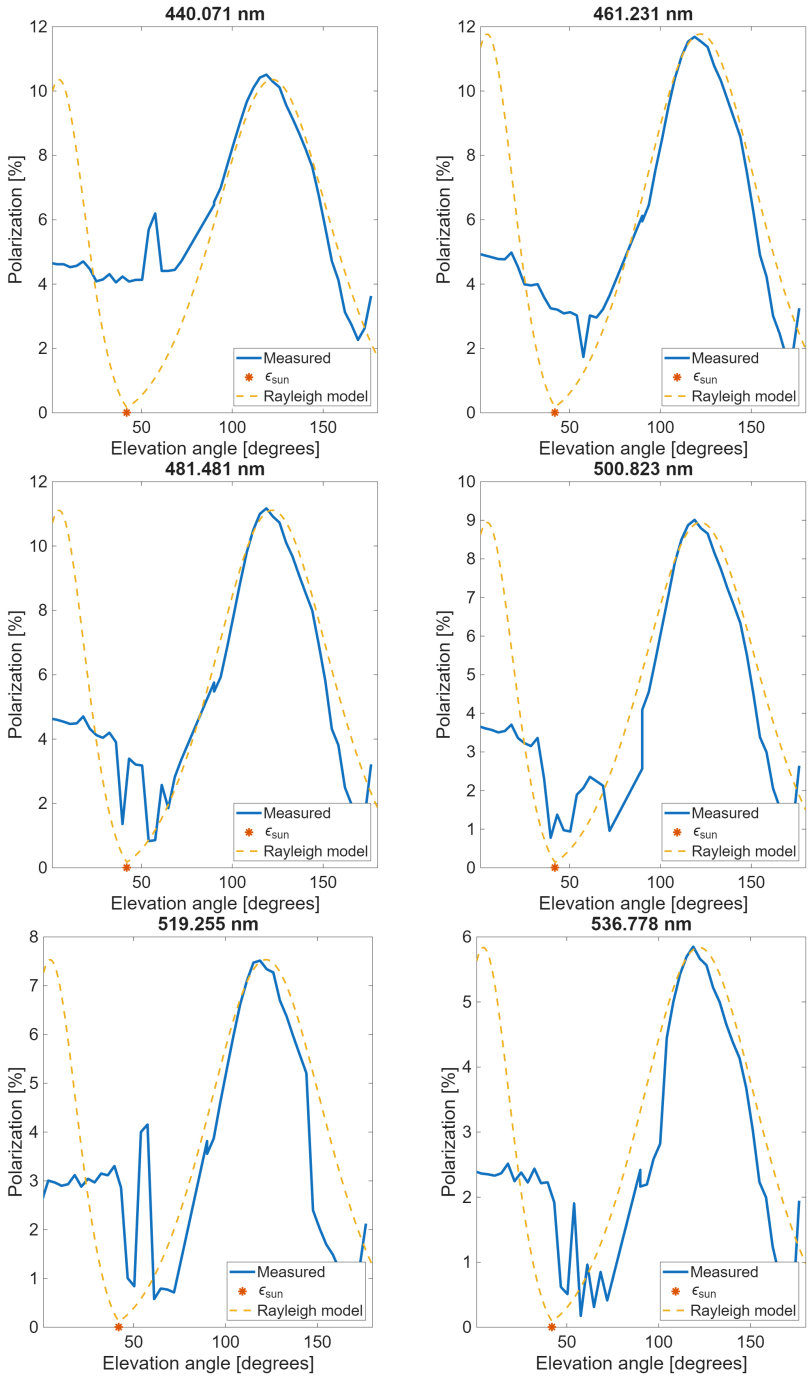

Figure 28: Principle plane measurements. The measured data does not drop to zero close to the sun, likely due to a positional deviation from the principal plane, existence of neutral points and buildings.

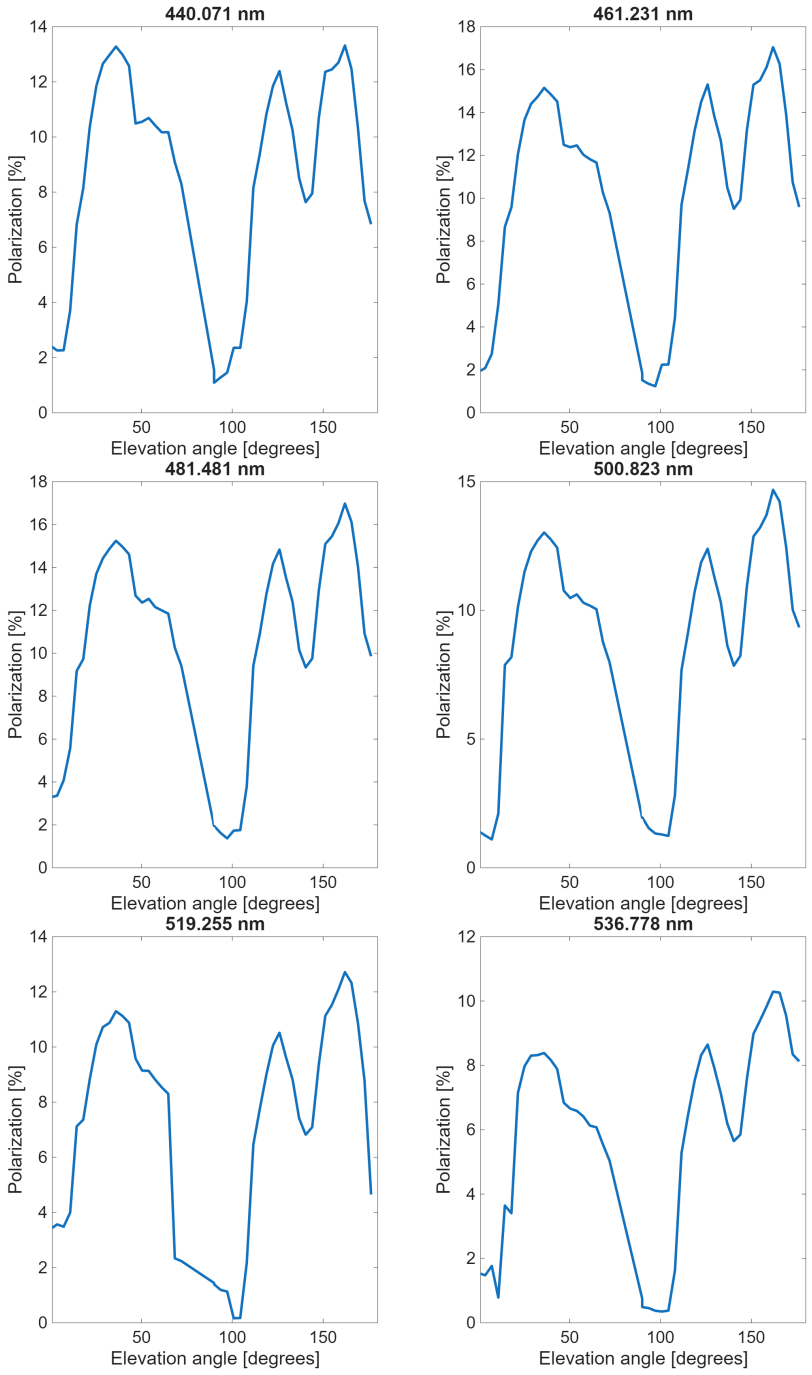

Figure 29: The direction of the sun relative to the plane of of measurement is 90 degrees so the bi-bell shape is as expected. A logical reason for the sharp dip at 140^o has not been found.

6.2 Smoke plume measurements

A search was conducted by car in western Sweden, close to Gothenburg, in areas of industry after suitable smoke plume targets for field measurements. Several pulp mills were identified as producers of steady smoke plumes of size sufficient enough to likely be detectable. The instrument was taken to one of these mills on a few days of clear weather. The content of the emissions had been publicized which meant that good reference material is available for future analysis of the data [**30**]. The instrument was placed outside of the industrial perimeter at a distance of a few hundred meters. The hypothesis to be tested was that the degree of polarization should undergo a distinct and sharp decrease when retrieved from the direction of the smoke plume relative to the blue sky beyond.

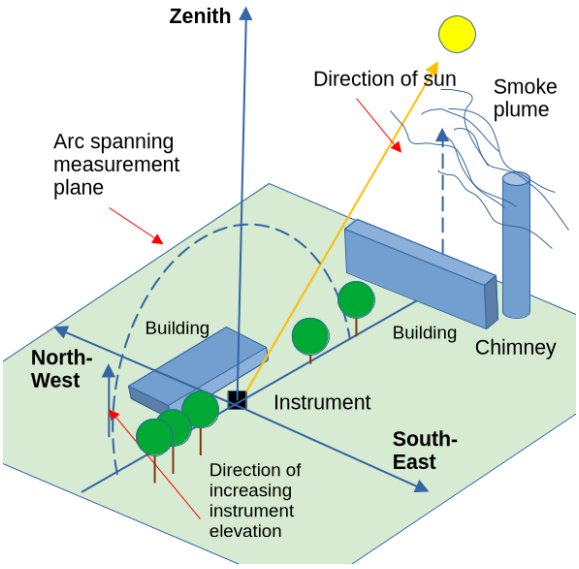

(a) Schematic of field measurement.

(b) Image of pulp mill and instrument direction. Note that the instrument only catches light falling parallell to the aperture direction so the chimney should not interfere with the measurement. The instrument was horizontal so the tilt is due to the camera.

Figure 30: Pulp mill measurement environment.

No official recourse regarding chimney height were found and no response from contact with the mill company had been received at the time of writing but a study visit report place the chimney at 120 meters tall, which seem realistic [**31**]. Measuring from google maps the chimney was about 200-250 meters from the measurement position, placing the elevation angle of the smoke plume at about 25 degrees. The measurement environment is visualized in figure 30. The orientation of the instrument relative to the sun was such that the measurement would be in the principle plane.

6.2.1 Results

The results of the measurements can be seen in figure 31. The distinct drop in polarization exactly where the approximate base of the plume is located, is likely due to the influence of the plume since it persists between measurement series and wavelengths. The small peak below the presumed plume base is likely due to the blue sky visible between the plume and the buildings below. The mechanism of the drop is probably a combination of the light scattered from the plume being less polarized when reflected directly and that the transmittance of polarized light from the sky in the background is at least partly blocked. That we do not see a drop to zero could be due to some polarized light getting through, that light scattered by the plume could become polarized to some degree, a polarization floor produced by the effect of the rotating mirror, or that the resolution of the measurement not being high enough to detect the drop.

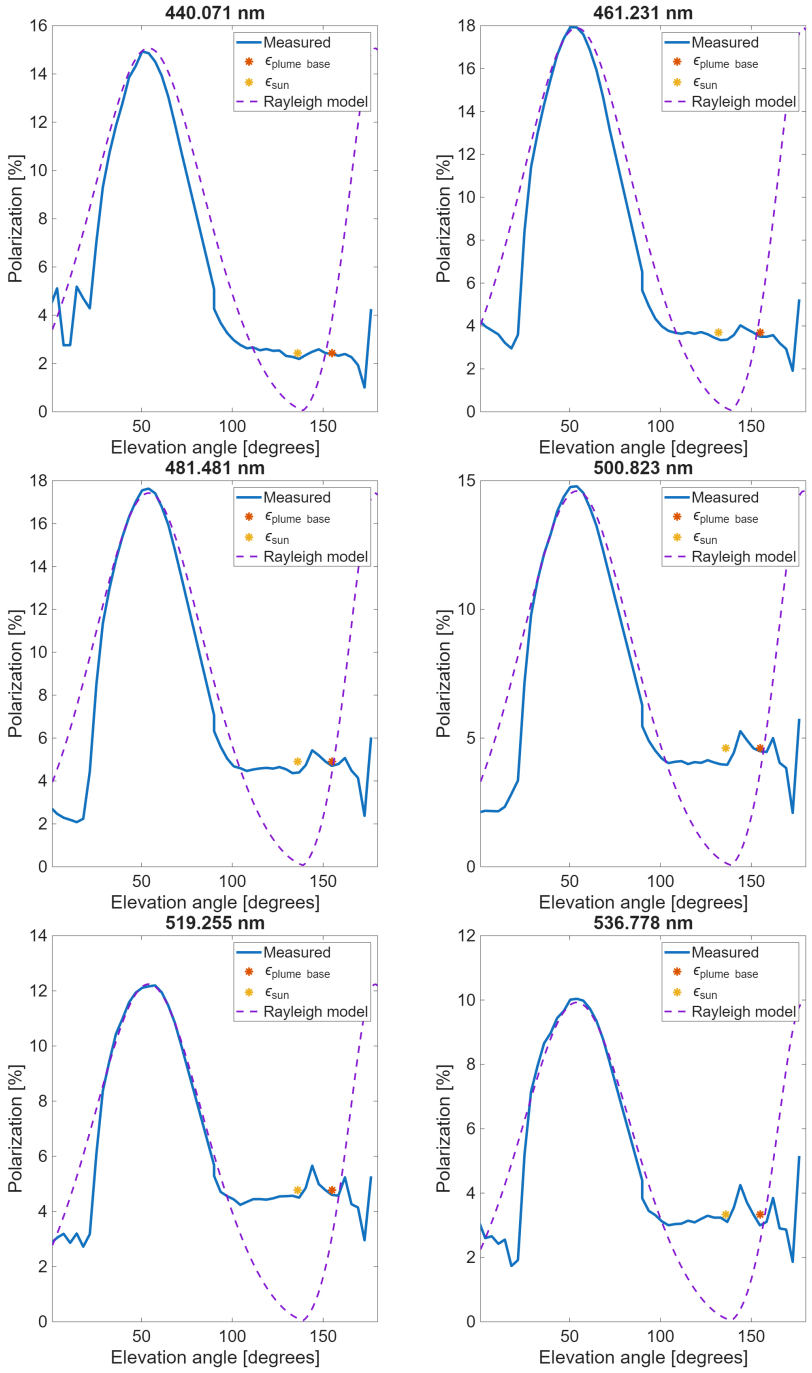

Figure 31: Polarization curves from measurements of smoke plume from pulp mill plant. The yellow star indicates calculated elevation of the base of the plume. The red star indicates estimated elevation of the sun.

7 Summarizing conclusions

The aim of building a prototypical device capable of detecting the polarization of scattered light in a channeled way, was achieved. Importantly, the capacity of the prototype to detect the influence of a smoke plume on polarization under at least certain conditions has been demonstrated. The possible integration of a future version of this instrument into NOVAC has been facilitated through the instrumental assembly that was used.

This instrument does not provide the full spectra as SPEXone and groundSPEX does. Since we only get one of these instruments orthogonal component it lacks 50% of the information. However, the shapes of the spectra gathered seem to indicate that the capability of the instrument to detect large scale particle variations such as plumes by means of interpolation and small angle high resolution measurements, is robust.

The data processing method seem to produce results matching those of other studies of sky polarization, which indicates that it is robust for parts of the spectra with a good signal to noise ratio. This signal to noise ratio, which then sets the limit of the methods robustness was not quantized. It is clear that the method did provide non stable and wildly varying polarization diagrams for noisy parts of the spectra. The work to differentiate noise from depolarization peaks (or polarization minima) caused by presence of aerosols or similar has not been done and it is not clear to what extent this is possible with the solitary light path method. It is possible that a finer resolution measurement algorithm that decrease the angular interval would have brought more clarity for interpretation of the polarization curves retrieved.

The tests performed focus mainly on detecting variations in degree of polarization, however, the capability of the instrument to detect varying angles of polarization have also been demonstrated, perhaps most clearly in the "mirror influence test". The influence of the mirror has been assessed theoretically, but not quantized and verified through experiment.

8 Suggestions for further development

Multiple measurements of smoke plumes to assess the limits of the instruments capabilities in regards to opacity and varying distinction from background in the form of overcast skies or haze would be of interest. Higher resolution measurements, meaning shorter angle increments during field measurements, would provide higher resolution polarization diagrams and could make possible the resolution of angularly smaller depolarization sources in the measurement environment.

For the benefit of creating a full documentation of a future finished instrument, measurements of the attenuation factor and extreme limits of statistically detectable intensity could be relevant. Quantization and offset of the influence of the rotating mirror would be good to perform and include in the data processing algorithm.

A shorter telescopic tube could enable use of a shorter intermediary casing segment, which would decrease overall weight of the instrument.

The polarimeter casing design could benefit from a more easily reproducible mechanism for optical component fixation. One part of this is already included in the design in the form of parallel slots on the inside of the casing.

To fully scope the instrument's capabilities and the resolution limits, field measurements on other targets than industrial plumes could also be of interest. Other tests of the instrument could involve assessing the influence of varying ground based backgrounds on the profile of low elevation measurements or the influence of altitude on measurements. Repeat of measurements during overcast skies can be relevant since the degree of linear polarization is then lower, meaning that the average signal to noise ratio is expected to drop for identification of local depolarization sources.

The capability of the instrument to characterize specific aerosols through polarization remain to be tested.

9 References

[1] NASA Official: Werdell, Jeremy. 2025-02-13. "PACE: Plankton, Aerosol, Cloud, ocean Ecosystem". Available at `https://pace.oceansciences.org/spexone.htm` (Accessed 2025-02-16).

[2] Aaldert, A.van et al. 2018. "SPEXone: A compact multi-angle spectro-polarimeter". Proceedings International Conference on Space Optics, ICSO 2018, 9-12 October 2018, Chania, Greece.

[3] Harten, G.van et al. 2014. "Atmospheric aerosol characterization with a ground-based SPEX spectropolarimetric instrument". Atmos. Meas. Tech., 7, pp.4341–4351.

[4] NOVAC.No author. No date. "Novac, Network for Observation of Volcanic and Atmospheric Change". Available at `https://novac-community.org/` (accessed 2025-07-06).

[5] Ewart,P. 2019 "Optics", Morgan & Claypool Publishers, series pp.2053-2571, Chapter 11.

[6] Hecht, E. 2013. "Optics". Pearson education. 4th edition.

[7] Horváth, G et al. 2014. "Polarization of the sky", in Horváth, G et al, "Polarized Light and Polarization Vision in Animal Sciences". 2nd edition, pp.367-406. Springer Berlin Heidelberg.

[8] Pomozi, I; Horváth, G; Wehner, R. 2001. "How the clear-sky angle of polarization pattern continues underneath clouds: full-sky measurements and implications for animal orientation". Journal of Experimental Biology, 204(17):pp.2933-2942.

[9] Collet, E. 1984. "Measurement of the four Stokes polarization parameters with a single circular polarizer". Optics Communications, volume 52, number 2, pp.77-80, issn 0030-4018.

[10] Lockwood, D,J. 2016, "Rayleigh and Mie Scattering", Encyclopedia of Color Science and Technology. Springer Berlin Heidelberg, pp.1097-1107.

[11] Nousiainen, T, et al. 2012. "Comparison of scattering by different nonspherical, wavelength-scale particles". Journal of Quantitative Spectroscopy and Radiative Transfer, Volume 113, Issue 18, pp.2391-2405.

[12] Cronin, T,W and Marshall, J. 2010. "Patterns and properties of polarized light in air and water". Phil. Trans. R. Soc. B (2011) 366, pp.619–626.

[13] Fesenkov, V,G. 1961. "The presence of elliptical polarization in the light of the day sky". Soviet Astronomy, vol 4, nr 5, pp. 741-884, translated from original published in vol 37, nr 5, pp.785-944, 1960.

[14] Zubko, E,S. . 2012. "Light scattering by irregularly shaped particles with sizes comparable to the wavelength". In: Kokhanovsky, A. (eds) Light Scattering Reviews, Vol. 6. Springer, Berlin, Heidelberg. p.57.

[15] Hansen,E., Travis, L.D. 1974."Light scattering in planetary atmospheres". Space Sci Rev 16, p.542.

[16] Collet, E. 2005. "Field guide to polarization". SPIE—The International Society for Optical Engineering, Vol FG05.

[17] Smit, J, et al. 2019. "SPEX airborne spectropolarimeter calibration and performance," Appl. Opt. 58, pp.5695-5719.

[18] Honggang Gu et al. 2018. "Comprehensive characterization of a general composite waveplate by spectroscopic Mueller matrix polarimetry". Opt. Express 26, 25408-25425.

[19] Snik F., Karalidi T. and Keller C.U. 2009. "Spectral modulation for full linear polarimetry," Appl. Opt. 48, pp.1337-1346.

[20] Thorlabs. "Fresnel rhomb retarders". Available at https://www.thorlabs.com/newgrouppage9.cfm?objectgroup_id=154 (Accessed 25-06-23).

[21] B.Halle Nachfl. 2017. "Superachromatic retarders". Available at https://www.b-halle.de/products/retarders.html (Accessed 2025-06-23).

[22] Thorlabs. "GTH10M - Mounted Glan-Thompson Calcite Polarizer, 10 mm x 10 mm Clear Aperture ". Available at https://www.thorlabs.com/thorproduct.cfm?partnumber=GTH10M(accessed 2025-07-06).

[23] I. H. Malitson. Interspecimen comparison of the refractive index of fused silica. J. Opt. Soc. Am. 55, pp.1205-1208 (1965)

[24] Trevisi, R et al. 2014. "A comparison of radon and its decay products" behavior in indoor air". Radiation protection dosimetry, vol 162, no 1-2, pp. 171-175.

[25] Richard, C et al. 1996. "Physical characterization of incense aerosols". The science of the total environment, 193, pp.149-158.

[26] Sun, W. et al. 2013. "For the depolarization of linearly polarized light by smoke particles". Journal of Quantitative Spectroscopy and Radiative Transfer, Volume 122, pp.233-237.

[27] Zubko, E,S et al. 2001. "Light Scattering by Composite Particles Comparable with Wavelength and their Approximation by Systems of Spheres". Optics and Spectroscopy, Vol. 91, No. 2, 2001, pp.273–277.

[28] Adhiya , A, et al. 2021. "Determination of Mueller Matrix for Metal Substrates by Stokes Polarimetry". IEEE Transactions on Instrumentation and Measurement, vol. 70, pp.1-7.

[29] Emde, C et al. 2010. "The impact of aerosols on polarized sky radiance: model development, validation, and applications". Atmos. Chem. Phys., 10, pp.383–396.

[30] Södra. Värö. 2024. "Sustainibility data". Available at https://mypulpplus.sodra.com/sustainability/environmental/SWB/1806/V%C3%A4r%C3%B6/2024?reportType=All (Accessed 2025-06-23).

[31] Ringhalsveteranerna. Report of study Visit to Södra cell Värö. Available at https://rivet.se/RV_2017/2017-10-02_Studiebesok_Sodra_Cell_V%C3%A4r%C3%B6_2_okt_2017.pdf. Accessed 2025-06-15.

DEPARTMENT OF SPACE, EARTH AND ENVIRONMENT
CHALMERS UNIVERSITY OF TECHNOLOGY
Gothenburg, Sweden
www.chalmers.se

CHALMERS
UNIVERSITY OF TECHNOLOGY